

POLITECNICO DI TORINO

Department of Mechanical and Aerospace Engineering

Master's Degree in Mechanical Engineering

Master's Thesis

**Dynamic behaviour prediction of a
rotating shaft and an overhung bladed
disk assembly**



Supervisor:

Professor Maria Teresa Berruti

Candidate:

Fasani Francesco

December, 2020

Contents

1	<i>Introduction</i>	2
1.1	Aim of the work and premises	2
1.2	General rotordynamics considerations	2
1.3	Gyroscopic effect	5
1.4	Stress stiffening	7
2	Bladed discs and their dynamic behaviour	9
2.1	Classification of mode shapes	9
2.2	Modal analysis data interpretation	10
2.3	Rotating bladed discs	11
3	<i>FE codes Gyroscopic effect evaluation</i>	13
3.1	Stodola-Green rotor modelling	13
3.1.1	Lumped models	14
3.1.2	Explicit models	14
3.2	Results comparison	15
3.3	Chapter conclusions	17
4	<i>Blade effect evaluation on Stodola-Green model</i>	18
4.1	Bladed disc modelling	18
4.1.1	Model features	18
4.1.2	Modal results analysis	18
4.2	Bladed Rotor modelling	21
4.3	Model validation	22
4.3.1	Solver peculiarities	22
4.3.2	Dynamic behaviour of the blisc-shaft assembly with pitch angle of 90°	22
4.4	Evaluation of the influence of the blade pitch angle on the dynamic behaviour	26
4.4.1	Description of the model	26
4.4.2	Comparison of the different pitched assemblies behaviour	27
5	<i>Modelling of the propeller shaft assembly of the engine of the ATR-72</i>	32
5.1	General overview of the ATR72	32
5.2	General overview of open rotors technology	32
5.3	Propeller model	32
5.3.1	Material choice	34
5.3.2	Constraints setting	35
5.4	Dynamic behaviour of the ATR-72 assembly	36
6	Conclusion	41
7	Appendix	43
7.1	Ch.3	43
7.1.1	Stodola-Green <i>Matlab</i> lumped model personally written	43
7.1.2	FUNCTION TO ASSEMBLE MATRICES	44
7.1.3	FUNCTION TO DECOUPLE AND SOLVE THE SYSTEM	44
7.1.4	Stodola-Green <i>Ansys APDL</i> lumped model	45

7.2	Ch.4	49
7.2.1	Solution routine for the pre-stressed rotordynamic analysis of the bladed disc-shaft assembly	50
8	RINGRAZIAMENTI	55

Abstract

One of the most important challenges of our century is ensuring, as engineers, the design of the most sustainable machines guaranteeing anyway the right amount of performances. A clear example of this topic comes from the aeronautical field where it is possible to observe the will to push for an increase of weight reduction and aerodynamic efficiency, which lead to energy savings and performance increment. An effort in this sense has been made for what concerns the engine design in an open rotor configuration. An example of this trend is found in the increase of adoptions of propfan engine. In fact, this architecture can be more efficient from the aerodynamic and thermodynamic point of view. On the other hand, the open rotor configuration and the goal of weight reduction lead to a flexibility increase of the engine parts. A particular focus is put on the bladed disc-shaft assembly. In fact, despite the classical approach for the study of the engine dynamics, which provides the analysis of each component separated, neglecting the Gyroscopic effect, the new trend goes towards a "whole engine philosophy design" analysis [1]. This new way of working is exploited, in this thesis, in order to evaluate the behaviour of a bladed disc shaft assembly. A particular focus is put on the influence of the phenomenon of the gyroscopic effect.

To pursue these objectives, some benchmark models of a Stodola-Green rotor have been realized through different codes (*Ansys* and *Dynrot student version*) in order to understand and compare how the different codes handled the problem. After this step, another simple model was realized in order to fully understand the dynamic features added to the system by including blades to the disc of a Stodola-Green model and, making the pitch angle change. In the final stage, the work is centred on the rotordynamic modelling, through FE, of the behaviour of a lightweight propeller of an ATR-72 mounted on his shaft.



Figure 1: ATR-72

1 Introduction

1.1 Aim of the work and premises

The aim of the work is analysing, exploiting FE capabilities, the dynamic behaviour of a rotating shaft with an overhung bladed disc. In particular the focus is on the the assessment of the influence of the gyroscopic effect on the rotor and of the change in the pitch angle of the blades. The analysis is a rotor dynamic one in order to evaluate the critical speeds, mode shapes and possible instabilities which could affect the life and the correct functioning of these components which are the main parts of an open rotor engine. Particular attention is dedicated to the study of the flexural modes of the blades which , as the evolution of the engine continues, are becoming longer increasing their flexibility. In order to understand how to correctly represent all these situations in a finite element environment, the process has started with the creation of simple models of Stodola-Green rotor. At these models have been added the complications of the blades and of the variability of the pitch angle. These example are taken as the starting ones because the work has begun with the analysis of [1] and the replication of its results. At the end, in order to try something tangible, a simplified model of the shaft-propeller assembly of an ATR-72 was analyzed.

1.2 General rotordynamics considerations

For what concerns the rotor dynamics study, it is reasonable to say that it is an expansion of the dynamic analysis in which is inserted another hypothesis that is the revolution of the part. In fact, if for example, for a dynamic analysis we start from an equation of the type:

$$[M]\{\ddot{x}\} + [C]\{\dot{x}\} + [K]\{x\} = 0 \quad (1)$$

where $[M]$ is the mass matrix, $[C]$ is the damping matrix and $[K]$ is the stiffness matrix, x is the vector of the degrees of freedom . On the other hand, the equation describing the free behaviour of a rotating system is:

$$[M]\{\ddot{x}\} + [[C] + [G(\Omega)]]\{\dot{x}\} + [[K] + [H]]\{x\} = 0 \quad (2)$$

where $[G]$ is the Gyroscopic matrix depending on the rotational speed and $[H]$ being the circulatory matrix. In principle what is possible to extract from the 2 systems is , in the first case, the eigenvalues of the system from which can be extracted the mode shapes, whose mathematical expression is related to the eigenvectors. Moreover, for what concerns the rotordynamic case formulation 2, it is possible another time to extract the eigenvalues which, this time, do not represent just the frequency of vibration at standstill but the whirling frequency, during the system rotation, in their complex part and, the decay rate in their natural part. In fact the eigenvalues in natural coordinates are expressed as:

$$\omega = \omega_w + i\omega_i \quad (3)$$

where ω_i represents the decay rate of the free motion of the rotor and ω_w the whirl frequency. Being the solution of the type:

$$x = x_0 e^{i\omega t} \quad (4)$$

which becomes:

$$x = x_0 e^{(-\omega_i + i\omega_w)t} \quad (5)$$

Instead if the eq. 2 was solved in the Laplace domain the solution would be of the type

$$x = x_0 e^{st} \quad (6)$$

where

$$s = s_r + is_i \quad (7)$$

and the whirling frequency is represented, this time, from the s_i whereas the decay rate by s_r . To note that since through this methodology of solution a state space system is used, the output will be directly the eigenvalues while, in the previous method the results were given in terms of the square of the eigenvalue. The whirl frequency mentioned opens the important topic of the definition of the whirl. In fact, considering a simple Jeffcott rotor which is described by the possibility of moving just in the plane along the x and y direction, the whirl motion is represented as the orbit coming out from the deflection of the shaft or of the supports of the shaft. This is due to the problem that, usually, for manufacturing reasons the center of gravity (G in fig. 2) does not coincide with the geometrical center of the the rotor giving birth to an orbital motion like in figure 2.

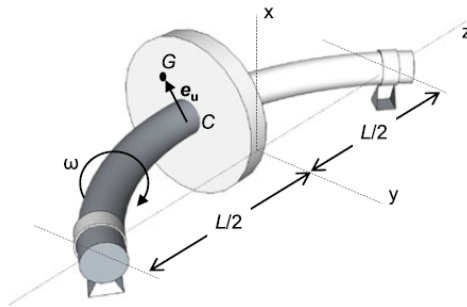


Figure 2: Jeffcott rotor deflection due to whirl motion

Moreover, there are some other distinctions to do about these whirl motions since they are of two different types:

- forward whirl;
- backward whirl.

The difference between these two cases is the direction of the whirl speed: in the FW the whirl motion happens accordingly to the angular velocity rotation direction, in the BW the whirl motion occurs in the opposite direction with respect to the rotational speed (around the main rotation axis). Moreover, it is possible to distinguish between cylindrical and conical whirl modes. The first ones are described as a whirl (circular or elliptical depending on the properties of the rotor/stator) with the axis of the rotor always parallel to the fictitious axis passing through the center of the orbit. In the conical whirling instead the axis of the rotor is no more parallel to the fictitious axis passing through the center of the orbit (figure 3).

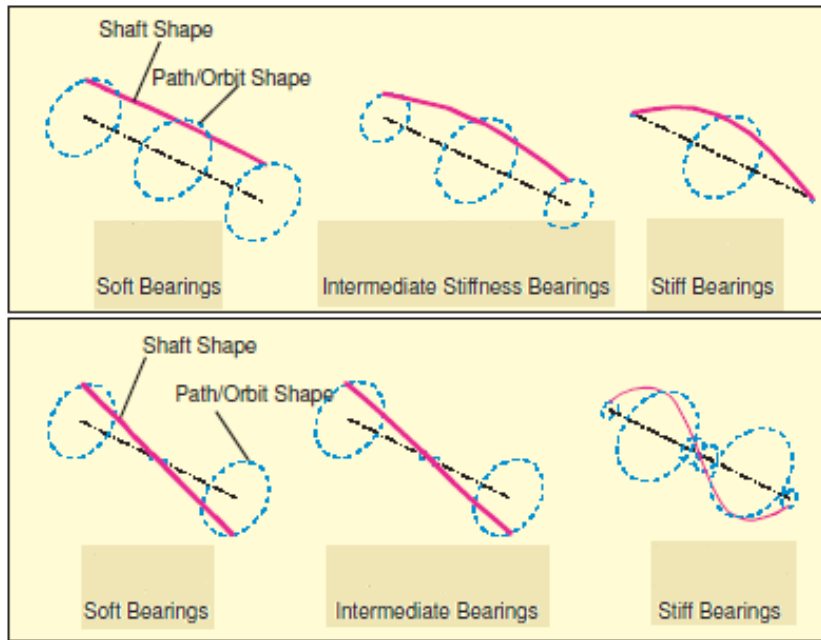


Figure 3: Cylindrical and Conical whirling [2]

Another peculiar thing adopted to describe in a easier way the whirl motion is the complex coordinate z , which in the xy plane describes the whirl orbit conjugating the x and y displacement through the expression [7]:

$$z = x + iy \quad (8)$$

which applied to the solutions becomes:

$$z = z_0 e^{i\omega t} \quad (9)$$

From the modulus of z in fact, as logical, it is possible to extract the orbit of the center of the rotor C . From the analysis of the behaviour of the whirl frequencies, as the revolution speed changes, it is possible to obtain a diagram called Campbell diagram (figure 4). This diagram help us to identify the critical speeds and the different mode shapes.

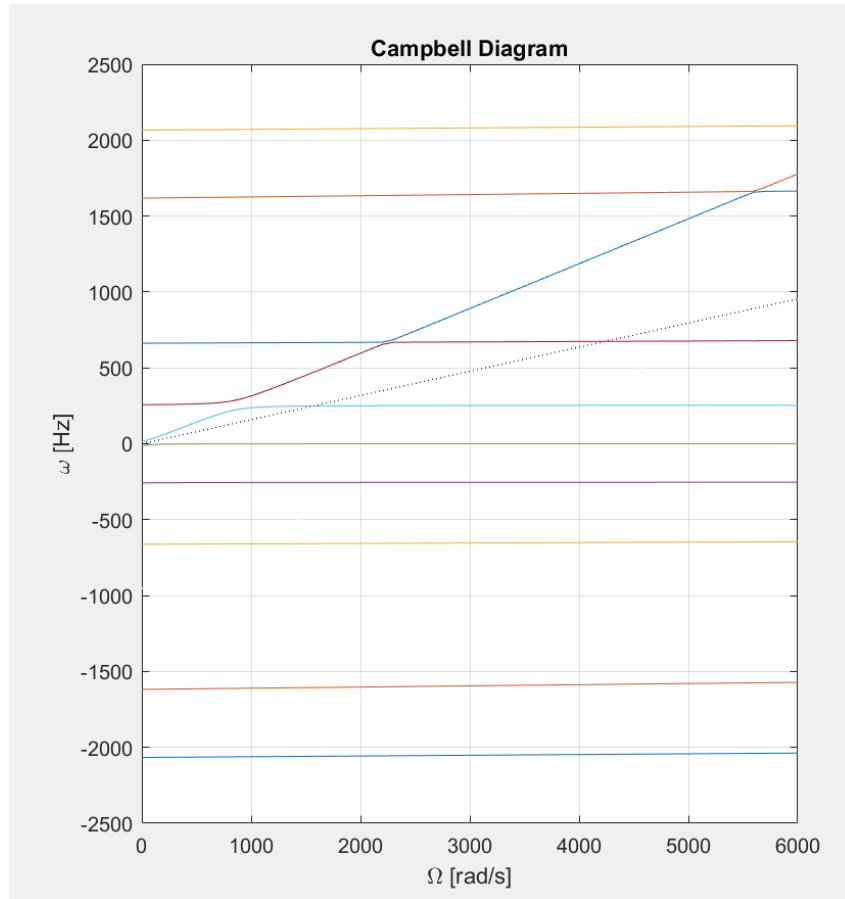


Figure 4: Campbell diagram example

The critical speeds are the speeds for which the response to the excitation keeps growing linearly as time passes. It is spotted just for the FW motions and to assess the values of these frequencies (in an inertial reference frame), it is found the intersection between a line $\omega_w = k\Omega$ and the forward whirl curves. k is usually equal to 1 (dotted line figure 4) but, generally, it is chosen with respect to the frequency of an harmonic excitation acting on the system (and with excitation frequency multiple of the rotational speed or multiple of some particular features of the geometry). For what concerns, instead, a Campbell diagram plot in the rotating reference frame, the critical speeds are identified immediately by the intersection of the FW curve with the x axis. Another problem affecting the functioning of the rotor are the instability fields: these zones are found when the component of the eigenvalue ω_i is negative or becomes negative or, in the Laplace Domain, when s_r becomes positive. In fact, if this condition is satisfied, the growth of the orbit becomes exponential bringing the system to a really dangerous condition.

1.3 Gyroscopic effect

The Gyroscopic effect is a direct consequence of the Coriolis acceleration acting on the rotor

$$\mathbf{a}_c = 2\boldsymbol{\Omega} \times \mathbf{v}_r \quad (10)$$

where v_r is the velocity vector of one point of the non inertial reference frame (rotational reference frame). The consequence is the generation of a torque acting on the system 5.

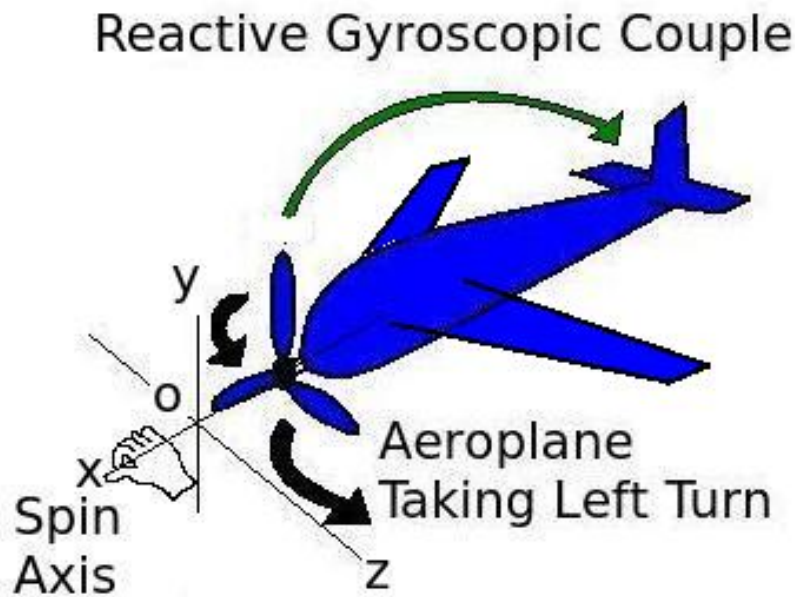


Figure 5: Torque applied by the gyroscopic effect during a turning maneuver

In rotors this happens when the axis has more components of rotational speed: in other words the Ω vector has not just the component around the rotation axis but also around the other two. The physical consequence of this phenomenon is the generation of a torque which tries, if the rotor is adequately designed, to re-align the shaft along the principal rotation axis. In some other cases it could bring to a further destabilization of the system and even to rupture. Anyway the shaft is subjected to a flexural action.

Considering the effect of the Gyroscopic phenomenon on the rotor frequencies it is important to highlight a parameter which is called δ and is equal to the ratio between J_p (polar mass moment of inertia of the rotor) and J_t (transversal mass moment of inertia of the rotor). In terms of effect on the Campbell diagram ([3]):

- $\delta < 1$ (long rotor) yields to the identification of a critical speed (intersection of the FW curve with line $\omega = \Omega$), linked to the conical whirling;
- $\delta > 1$ (disc rotor) let the system avoid critical speeds (this at least for what concerns critical speed given by the intersection of the FW curves with the line $\omega = \Omega$);
- if $\delta = 1$ (spherical rotor), the system never reaches the critical speed but, in this way, the excitation on the system keeps growing in time as a sort of instability.

Accordingly, the effect on the frequencies behaviour gives no straight lines in the Campbell diagram (apart from the case in which $\delta = 0$ and the Gyroscopic effect is neglected) [3]:

- the frequency of BW whirling decreases in absolute value and tends to 0 as Ω goes to infinite;
- the frequency of FW whirling grows following the asymptote $\omega = \delta\Omega$.

It is possible to claim at the end, that the effect of the Gyroscopic phenomenon is a stiffening one. For example, in the case of the Stodola-Green Rotor, the Coriolis effect splits the complex conjugate frequencies, as shown in figure 6.

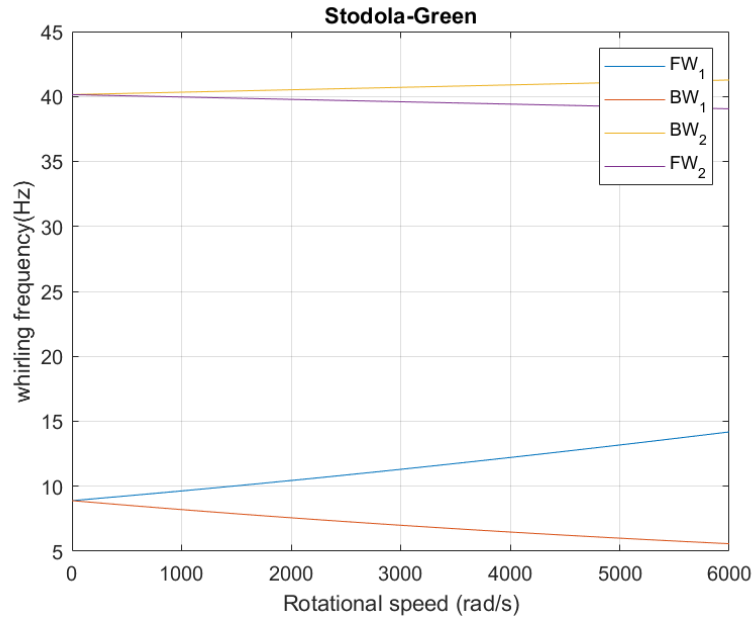


Figure 6: Campbell diagram showing the frequency split due to the Gyroscopic effect

As previously said, in figure 6 it is possible to appreciate the frequency split between the forward and backward whirl modes in absolute value.

1.4 Stress stiffening

Given a beam under an axial stress, its bending frequency of vibration (11) will be higher or lower depending on the fact that the stress is a stretching or a compressive one. The formula demonstrating the previous concept is taken by [7]:

$$\omega = \frac{i\pi}{l} \sqrt{\frac{EI}{\rho A} \left(\frac{i\pi}{l}\right)^2 + \frac{Fz}{\rho A}} \quad (11)$$

where:

- I, A, l are respectively the moment of area of the section of the beam, the area of the beam, the axial length;
- ρ is the density of the material;
- Fz is the axial force;
- i is the number of the mode shape.

Considering a rotating system, a feature, always characterizing, will be the presence of a centrifugal field given by the centrifugal force. This induces on the rotor a positive stress field

which is reflected into an increase of the frequencies: this phenomenon is represented in the field of the finite elements by the Geometric stiffness matrix. In the case of the stress stiffening effect caused by the centrifugal force field, the matrix is proportional to the spin speed because the centrifugal force has in its expression a dependence coming from it. At the end, the previous equation of the rotating system becomes:

$$[M]\{\ddot{x}\} + [[C] + [G(\Omega)]]\{\dot{x}\} + [[K] + [K_G(\Omega)] + [H]]\{x\} = 0 \quad (12)$$

In order to be consistent with the formulation of many commercial codes, it must be said that another effect influencing the stiffness of our system is present: the effect is called spin softening and acts differently depending on the reference system chosen (inertial or non inertial). In our case will be related to the centrifugal field force and so to Ω . At the end the equation comes out as:

$$[M]\{\ddot{x}\} + [[C] + [G(\Omega)]]\{\dot{x}\} + [[K] + [K_G(\Omega)] - [K_S(\Omega)] + [H]]\{x\} = 0 \quad (13)$$

where $[K_S]$ is the spin softening matrix.

2 Bladed discs and their dynamic behaviour

A common method to model bladed discs and in general cyclic symmetric structures exploits this symmetry around an axis in order to save computational efforts and time. In fact, the method consists in modelling just one sector and extending the result to the others. This can be done both for what concerns the static analysis and for the dynamic one.

2.1 Classification of mode shapes

From the theory of the axialsymmetric structures, if a mode has the maximum deflection point at some point on the structure, it is possible to rotate the mode shape of any angle not changing the frequency of vibration. The same holds for Cyclic symmetric structures. In the dynamic field, which is the one interested by this thesis, the possible mode shapes for the solution of a cyclic symmetric structure modal analysis can be classified into 3 categories [4]:

- each substructure has the same mode shape as its neighbours and is described by the expression

$$u^j = u^{(j+1)}; \quad (14)$$

- each substructure has the same mode shape as its neighbours but is vibrating in antiphase and is described by the expression

$$u^j = -u^{(j+1)}; \quad (15)$$

- all other possible mode shapes.

The second class of modes can only exist if the number of sectors composing the cyclic structure is even. For the first and the second types, rotating the mode shape is useless since the same shape is obtained. So their mode shape description is made with just one eigenvector. The third class, instead, can be described by different mode shapes for following sectors. Moreover, as demonstrated in [4], the solution of this type of modes can be represented better using complex coordinates, coming from the linear combination of real orthogonal eigenvectors $\{u\}$ and $\{\bar{u}\}$ which are individually solution of the system. So the complex linear combination coming out from those solutions is:

$$\{z\} = \{u\} + i\{\bar{u}\} \quad (16)$$

Now it is possible to write a solution of the equation which takes into account the deformed vector $\{z'\}$ around all the sectors by the formulation:

$$\{z'\} = e^{-i\Psi} \{z\} \quad (17)$$

from which comes out the expression relating the displacement of the sectors:

$$\{z^{(j)}\} = e^{i\Psi} \{z^{(j-1)}\} \quad (18)$$

where Ψ is the so called phase angle which is a parameter connected to the delay of the mode shape with respect two subsequent sectors. Moreover, its expression is:

$$\Psi = \frac{2\pi n}{N} \quad (19)$$

where N is the number of the cyclic sectors and n is the number of the nodal diameters. The number of the nodal diameters is another number that takes into account how a mode repeats

equal to itself after a certain number of sectors: in fact n/N gives the number of substructures after which the mode shapes repeats equal to itself. It is also important to say that n (integer number) ranges between zero and $N/2$ (excluding $n = 0$), if the number of sectors is even, and from zero to $(N - 1)/2$ if the number of sectors is odd. Moreover, in order to give a physical meaning to these complex solutions [4], what represents the instantaneous deflected shape of the system is the real part of eq. 17. Then it is important to underline also that since $\{z\}$ is a solution of the system obtained by a linear combination of two complex solutions, also its complex conjugate will be a solution of the system. The difference between the two will be the rotation direction of the mode shape: the first clockwise, the second anticlockwise. So, in other words, the multiplicity of the solution will be 2 for this type of mode shape while, for the other two the multiplicity will be 1 since the solution is real.

2.2 Modal analysis data interpretation

In order to understand the behaviour of the bladed disc, what is commonly done is to plot a diagram relating the frequencies of the different mode shapes with their nodal diameter related parameter. In fact, usually, the modal analysis output of the commercial code provides this last parameter.

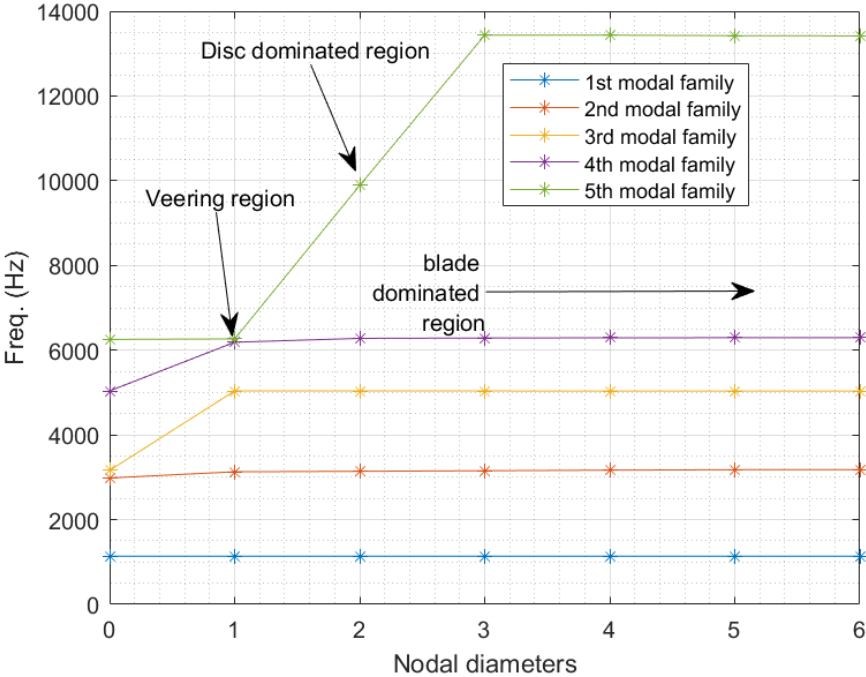


Figure 7: Modal families plotted with respect to nodal diameters

As shown in fig. 7, it is possible to distinguish between two different behaviours of the bladed disc: in fact depending on the frequency there is a major incidence of the movements of the blades 8 or of the disc 9. This behaviour is strictly dependent on the geometry of the system since for example, having a bulky disk and thin blades could cause the rise of only blade modes. On these types of graph it is possible to identify the areas dominated by disc modes since they present an increasing trend of the frequencies. On the other hand the blade dominated modes are identified by series of constant frequencies.

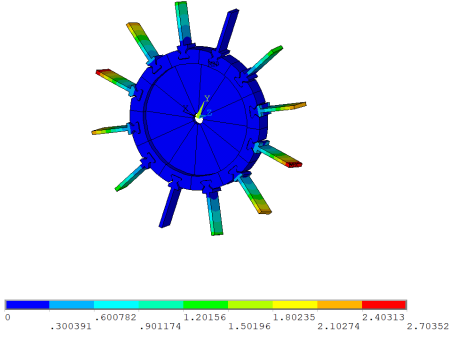


Figure 8: Blade mode correspondent to one nodal diameter

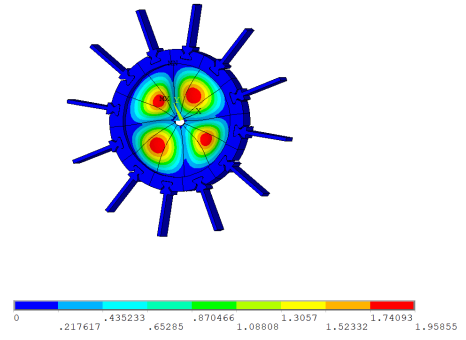


Figure 9: Disc mode corresponding to two nodal diameters

2.3 Rotating bladed discs

A good starting point for the study of a rotating part, attached radially to a disc, is the rotating pendulum. A basic and important point is the understanding of the difference between the in plane vibration of the pendulum and the out of plane one. In fact, they represent two ways of vibration, of the free pendulum, which are different starting from the mathematical expression of their frequencies [3]. Evolving the model, it is possible to write the expressions describing a rotating string attached to a disc. In particular, if the string is constrained to vibrate in a plane, it is found the dependence of the frequency from the angle Ψ between the axis of rotation and the plane [3]:

$$\omega = \sqrt{\omega_1 - \Omega^2 \sin^2 \Psi} \quad (20)$$

Moreover, ω_1 is the out of plane natural frequency of the string when it is free of vibrating and Ω is the spin speed of the rotor system. A particular feature to underline is that if $\Psi = 0$ a correspondence with an infinitely thin blade lying in the plane of the disc is found. The case is coincident with the one of out of plane vibrations while, if $\Psi = 90^\circ$ the scenario is the one of the in plane vibrations. Evolving another time the description of our model, leads us to have a description of a rotating blade attached to a disc : the beam taken into consideration is an Euler-Bernoulli beam which is slender and neglects the shear deformation and the kinetic energy of the cross section rotation about its axis [3]. A major characteristic of the mathematical problem, in this case, is that the solution depends strongly on the boundary conditions and so, on how the blade is constrained to the disc. The model shows, in analogy with the previous model, that if there is an angle Ψ between the rotation axis and one of the axis of symmetry of the beam (assuming the section of the beam as rectangular), the frequency will have a direct dependence on this angle and also a monotonic growth due to the spin speed. The natural frequency of vibration of the rotating beam attached to the disc is thus described by:

$$\omega = \sqrt{\omega_{in} + \Omega^2 (c_i - \sin^2 \Psi)} \quad (21)$$

Here (eq. 21) it is possible to notice how the frequency of the rotating blade is derived from an expansion of the standstill vibration frequency (ω_{in}). Moreover from the dynamic of the rows of rating pendulum chapter in [3], it is known that:

- in case of in-plane vibrations with no nodal diameter (commonly called nodal diameter 0) the bending behaviour of the blades is coupled with the torsional behavior of the shaft and disc composing the rotor;

- in case of out-of-plane vibrations with nodal diameter equal to 0 the bending behaviour of the blades is coupled with the axial behavior of the shaft ;
- for both out-of-plane and in-plane behaviour the nodal diameter equal to one exerts a bending excitation on the shaft ;
- the behaviour of the other mode shapes (with nodal diameter different from 0 or 1) is not influent on the dynamics of the rotor ;

If the blade, as commonly happens, is twisted, Ψ is not constant so the effect is a mix of the two. A step forward in the theory is made considering instead of a single entity pendulum or blade, a row of pendulums or blades evenly spaced and attached to a disc. From the results of the model reported at page 484 of [3], it is possible to understand, now, how the frequencies extracted describe a situation coincident with the modal analysis of the previous case which was in static conditions. In fact the row of pendulums are subjected exactly to the modes and the phase angles governed by the theory of the bladed discs. From the study of the interaction between the dynamics of a row of blades with the shaft in a rotor, it is found, numerically and experimentally, the rise of a instability region. The instability is detectable by the real part of the eigenvalue which becomes positive (Laplace convention) and is due to the presence of a geometrical ratio between the radius of the disc and the length of the blade, (or pendulum) which is minor than one. The phenomenon verifies just for the forward whirling mode (in the inertial reference frame) and has a worse effect when the angle Ψ is close to 90° or it is 90° since the speed for which rises are smaller. Instead, for the Ψ angle going towards zero, the effects are negligible since the birth of the instability is found for higher spin speeds. Anyway the instability verifies always in the supercritical field and, in the practical application, is usually not dangerous since the speed for which verifies cannot be reached for strenght related reasons of the materials adopted. On the other hand, because of the development of lighter and more resistant materials, the field of instability issue is a concept not to dismiss [3].

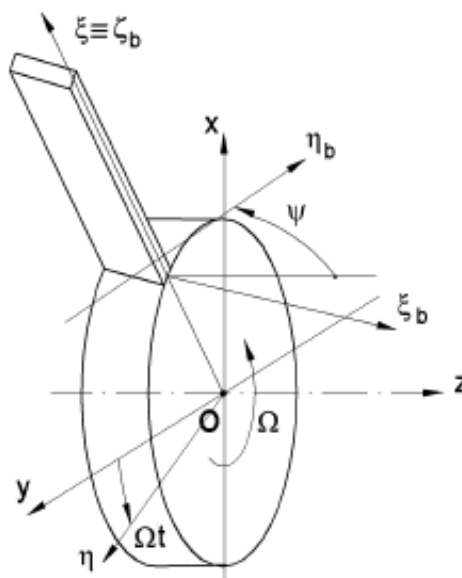


Figure 10: Rotating blade sketch (from [3])

3 FE codes Gyroscopic effect evaluation

As the mathematical methods and the hardware to perform the computations are being evolved, the approach to study the dynamic behaviour of engines becomes centered on the simulation of an always bigger part of the final assembly. This way of proceeding is the result of what is called "whole engine philosophy design"[1]. This allows in particular to take into account all the modes exchanges between a component and the other (for example between blisc and shaft connected) when the frequencies of the two are quite similar. In particular what gives value to this way of reasoning, which usually is closer to what happens in reality, is the need to model all the elements as elastic, neglecting the rigid body or rigid connections approximations [1]. At the end this way of proceeding is particularly important for our purpose since the open rotors design, with its increasing dimensions for what concerns the blades is particularly compliant as there is the will to go towards lighter structures.

3.1 Stodola-Green rotor modelling

In order to understand the peculiarities of the commercial code used (*Ansys*), for what concerns the rotordynamic analysis dealing with Gyroscopic effect, some benchmark models are here created to compare the results and try to replicate the numbers obtained in [1]. The example chosen for this "evaluation" of the codes is the well known "Stodola-Green" model which consists of a Disc attached to a cantilever shaft (which obviously can rotate around its axis). More than one modelling technique has been used in order to create this test (fig. 11):

- the first was written by myself on Matlab and it is a 2 complex degrees of freedom lumped model implementing the gyroscopic matrix (code in the Appendix, representation not present in fig. 11);
- the second model (still lumped) was obtained using a Matlab toolbox called 'DYNROT student version' which is a FE extension for rotordynamics (fig. 12);
- the third and fourth model were obtained using *Ansys Mechanical APDL* and they are constituted by a solid (fig. 13) and a lumped model (script in the Appendix);
- the last solid model was created employing *Ansys Workbench*.

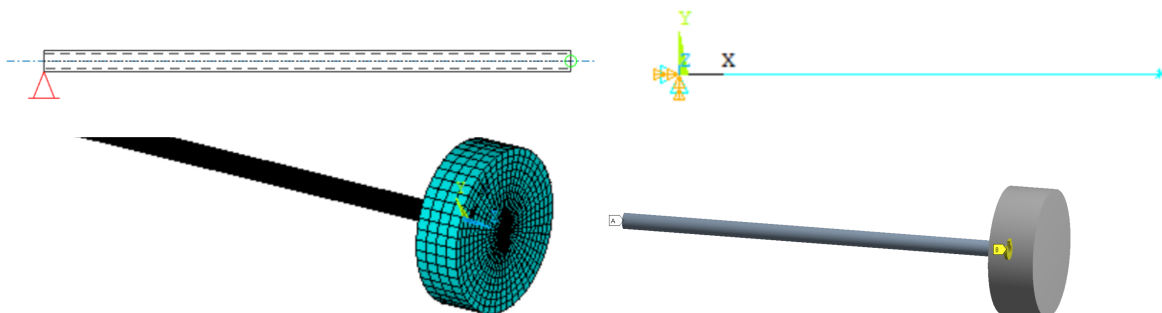


Figure 11: Starting from the left upper corner in clockwise order: Matlab 'DYNROT' model, *Ansys Mechanical APDL* lumped model, *Ansys Workbench* model, *Ansys Mechanical APDL* solid model

3.1.1 Lumped models

The lumped models used are the simplest available to simulate the case of the Stodola-Green rotors. They are both developed using Matlab and they are simply composed of 2 nodes connected by a beam. The nodes are employed, in one case to fix a concentrated mass (with mass moment of inertia to simulate the disc), and in the other case to set the cantilever constraints. A difference to underline is that the beams to simulate the shafts have 2 different formulations: in the first model a Euler beam was used while, a Timoshenko's one has been utilized through the *Dynrot* script. Moreover, the second model used was capable of developing a solution to the equation system with a professional mathematical solver able to operate in all cases in the field of the axial symmetric rotordynamic systems. Instead, the first model exploits the simplicity of its formulation: the solution in fact is obtained performing the modal analysis and Diagonalizing the system. At this point only decoupled equations are obtained and solved individually. The last lumped model, obtained using concentrated elements in *Ansys APDL* is the same as the other two, but this time it is obtained in a commercial software environment.

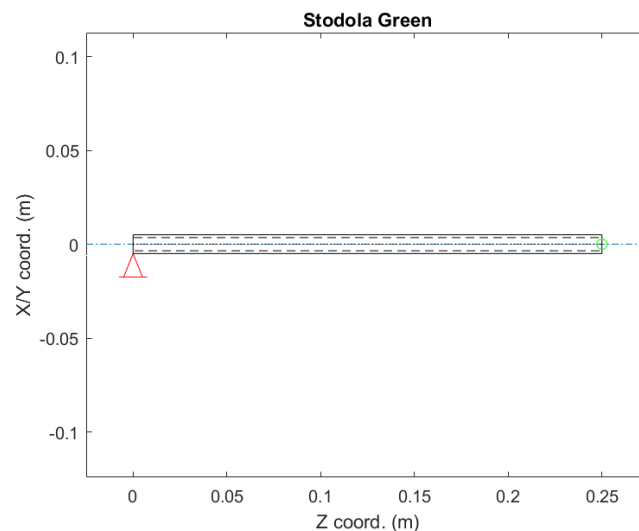


Figure 12: Lumped Stodola

3.1.2 Explicit models

The remaining models were created starting from a 3D CAD drawing. The mesh has been realised by employing solid elements such as 8 node brick element and tetrahedral elements. In the case of the 8 node element, implemented in *Ansys Mechanical APDL*, the mesh was realized with particular attention to the axial symmetry: for this purpose a sector has been meshed and then replicated (axially symmetric) in order to obtain the final shape 13. In the other model developed with *Ansys Workbench*, the mesh was completely delegated to the software, as well as the choice of the elements (as it is default for this environment). What came out, obviously, is a more irregular mesh due also to the fact that here the volume imported in the software was the entire one. The method of solution this time employs, in both the situations, the QR damped method which allows the calculations of complex eigenvalues. Another detail to mention is that, differently from [1] centrifugal stiffening has been neglected as well as spin softening.

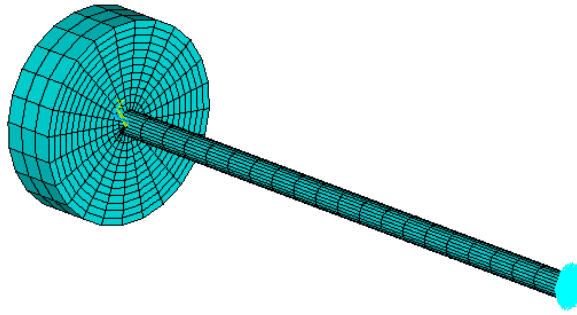


Figure 13: Solid model obtained through *Ansys APDL*

3.2 Results comparison

The term of comparison for the four different models has been the Campbell diagram for the two first whirling frequencies. It is possible to notice how the results are close to each other (fig. 14). So, for this geometry configuration, it is possible to appreciate how the different models formulations lead all to the same results (at least for what concerns the first family of whirling modes). As expected and showed in figure 14 the solid model brings with him a major

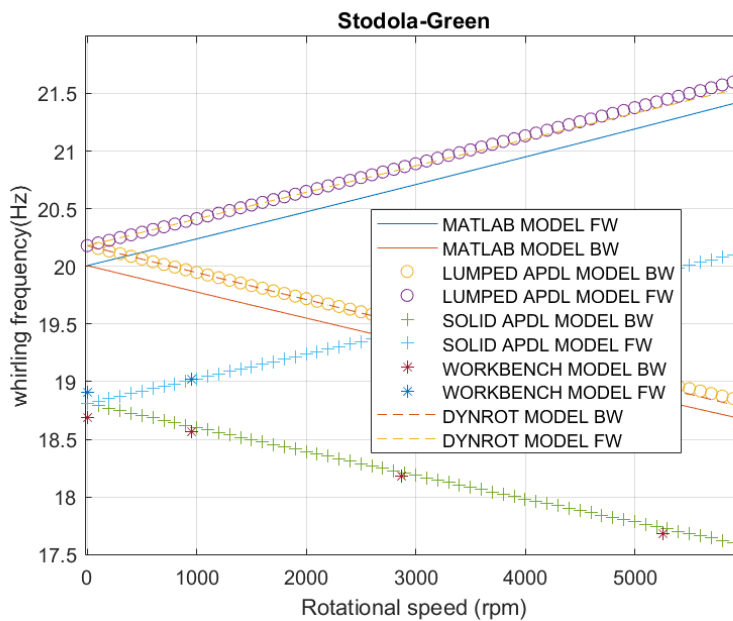


Figure 14: Campbell diagram in NON rotating reference frame

compliance with respect to the lumped one. This is due mainly to the shape functions of the elements which are of higher order compared to the one of the lumped beam. Another reason comes from the higher number of elements used in the discretization of the solid volume. Since for this study a really important starting point is constituted by the comparison also with [1], what comes out is the fact that for this geometry the effect of centrifugal stiffening (on the solid models) is negligible. This is due to the fact of the bulky profile of the disc which does not feel

so much the change in stiffness due to the centrifugal stresses. The proof of this is obtained in figure 15 where it is possible to see that there is no difference between the the pre-stressed configuration and the basic one. The little offset present between the 2 is of the order of the hundredths of Hz and can be associated to a small error in the numerical solver.

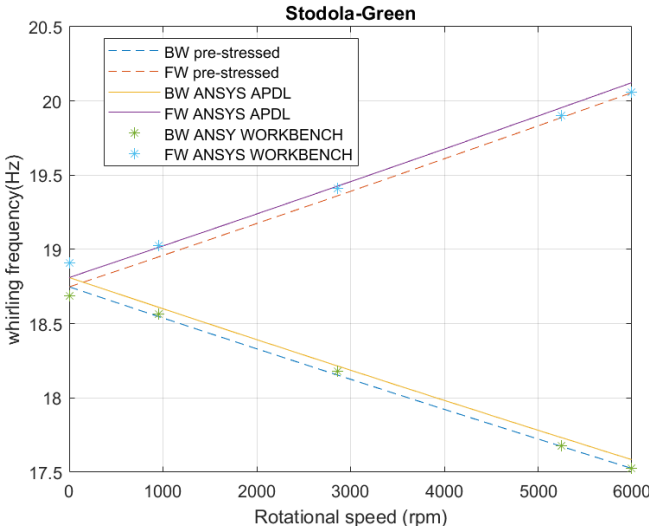


Figure 15: Campbell comparison among the pre-stressed case and the basic one

Moreover, another possible of the configuration of the Campbell Diagram can be plot in the rotating reference frame as shown in [1] and in figure 16. The choice of this type of graph allows to immediately identify the critical speed (around 1200 rpm) which is in correspondence of the drop of the branch below.

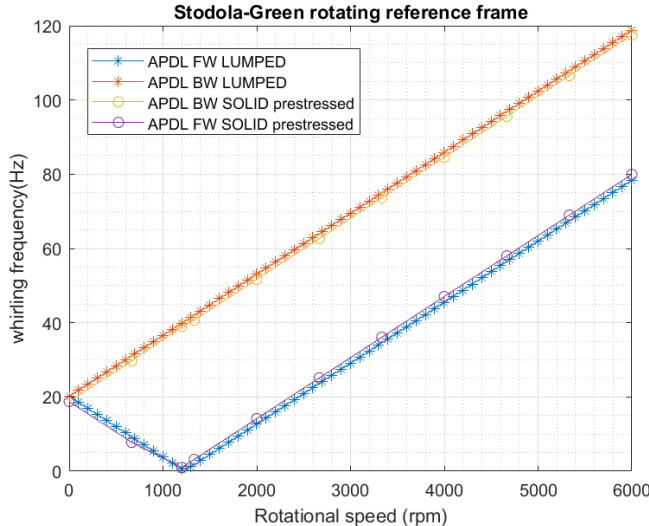


Figure 16: Campbell diagram in the rotating reference frame

3.3 Chapter conclusions

In conclusion, for this type of system it is possible to obtain similar results both employing minimal models, like the lumped models, in which are used few elements and nodes, both using solid element models. It is always important to evaluate if the geometry to represent is bulky enough to neglect the centrifugal stiffening and the spin softening.

4 Blade effect evaluation on Stodola-Green model

Since our final target is the understanding of the dynamic behaviour of a propeller-shaft assembly of a turboprop engine, a good way to start is with a simple model. In particular the choice has fallen on the introduction of some blades on the disc of a Stodola-Green rotor (fig. 23). In this process another important parameter to take into account is the pitch angle, or in other words, the angle between the chord line of the blade and the plane of the axis of rotation of the shaft. In fact, it is important to have an idea of the frequency changes as the pitch angle varies since, such a technique is adopted in to satisfy the aerodynamic requirements, during the different phases of the flight.

4.1 Bladed disc modelling

Before even start to think to the analysis of the rotor, it is intelligent to run a modal Analysis of the bladed disk in order to understand its dynamic behavior. In fact, as said in [3] in the part regarding the dynamic of the rows of pendulums, the blisc dynamic influences a lot the one of the rotor. Moreover, this blisc model is similar to the one described in the ideal case (which has a rigid disc with attached pendulums) since features a bulky disc and thin blades.

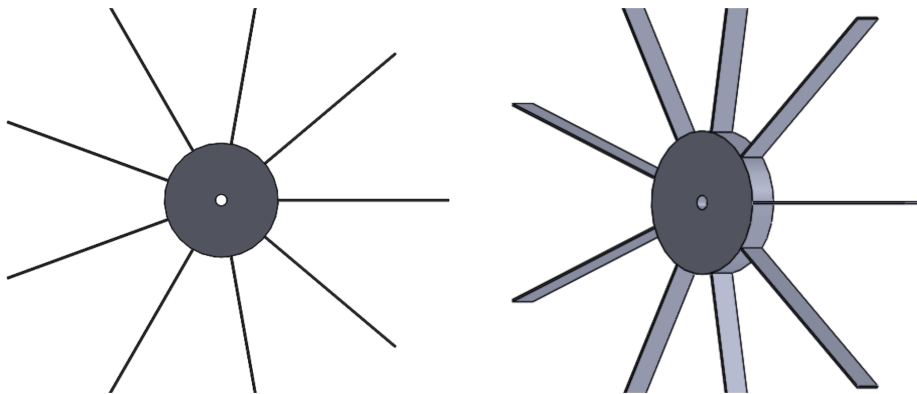


Figure 17: Bladed disc

4.1.1 Model features

In order to describe the bladed disc, a model exploiting the circular symmetry has been created. Such a way of proceeding helps to find directly a solution to the modal analysis (in *Ansys APDL*) which takes into account the nodal diameters.

The only particular thing to mention is that, to simulate the constraint of the shaft, the degrees of freedom of the circular crown of the hole in the center of the disc have been locked.

4.1.2 Modal results analysis

From the data obtained from the modal analysis it is possible to characterize the blisc.

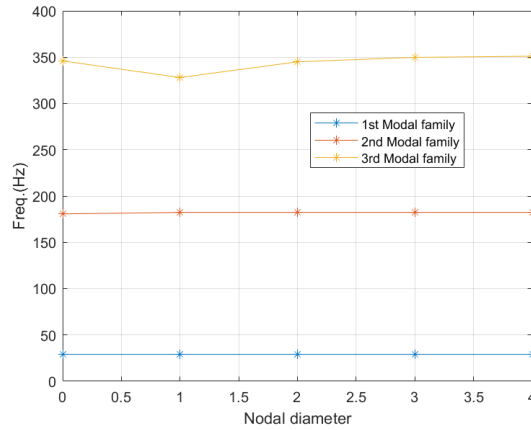


Figure 18: Frequencies of the disc as the nodal diameter varies

In figure 18, it is possible to notice as the frequencies, for the first three modal families, remain the same as the nodal diameter changes. This is index of the non participation of the disc to the mode shape: in fact all these 3 families are constituted by blade modes. This happens because of the thick profile of the disc with respect to the blades. Moreover, as expected, the number of nodal diameters is 4 (excluding the zero nodal diameter): the solutions are complex and conjugate for Nodal diameters from 1 to 4, while the Zero nodal diameter brings a real solution.

More than the image plot of the modal shape it is important to have something numerical in order to find out the behaviour of the mode shape. This tool of comparison is constituted by the plot of the angular displacements of the tip of the blade and, is useful to spot the participation of the blisc to the total mode shape of the rotor in the following section analysis.

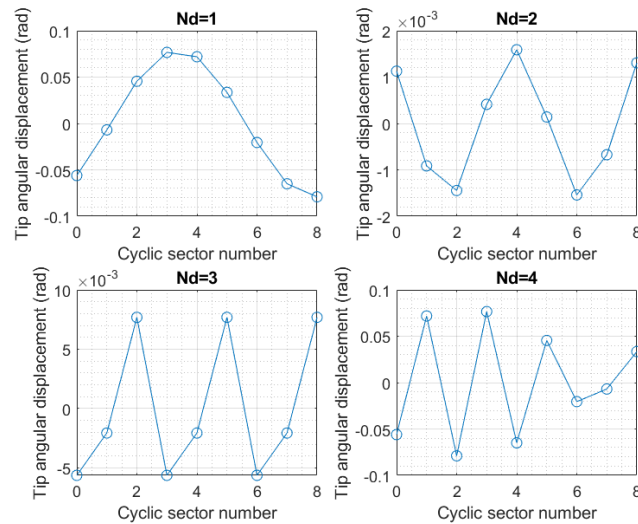


Figure 19: Tip displacement diagram for each cyclic symmetric sector of the blisc in the 1st modal family (all these modes of blade are at 29 Hz as shown in fig. 18)

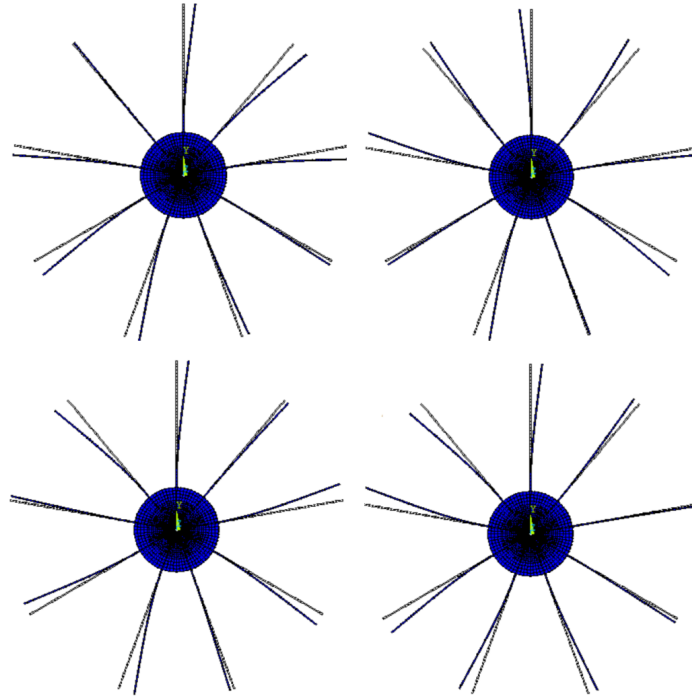


Figure 20: Mode shapes (1st modal family) of the previous tip displacement plots (starting from the upper right in clockwise order $Nd = 1, Nd = 2, Nd = 4, Nd = 3$)

As it is possible to notice (fig. 19) the tip displacement, represents just a rough indication of the nodal diameter, since, having an odd number of sectors, the cyclic symmetry cannot be 'cut' in equal pieces having inside the same number of sectors: thus the tip displacement curve can not be related strictly to the periodicity of the nodal diameters. Anyway, the plots from $Nd = 1$ to $Nd = 3$ give the idea in a pretty precise way of the corresponding nodal diameters since the number of intersections with the X axis are the right ones. The last mode shape missing is the one describing the Zero nodal diameter.

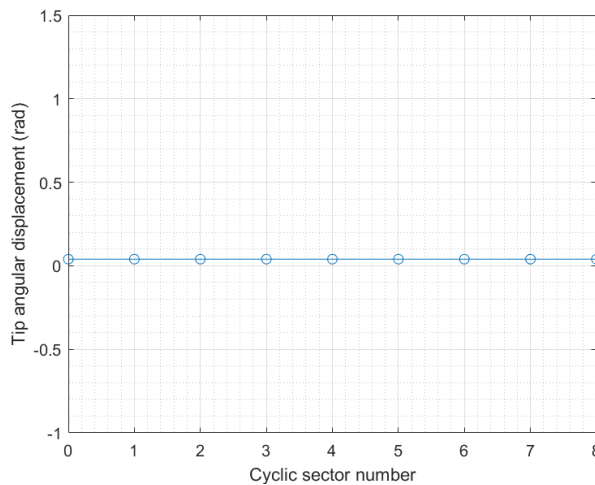


Figure 21: Zero nodal diameter plot tip displacement at 29 Hz

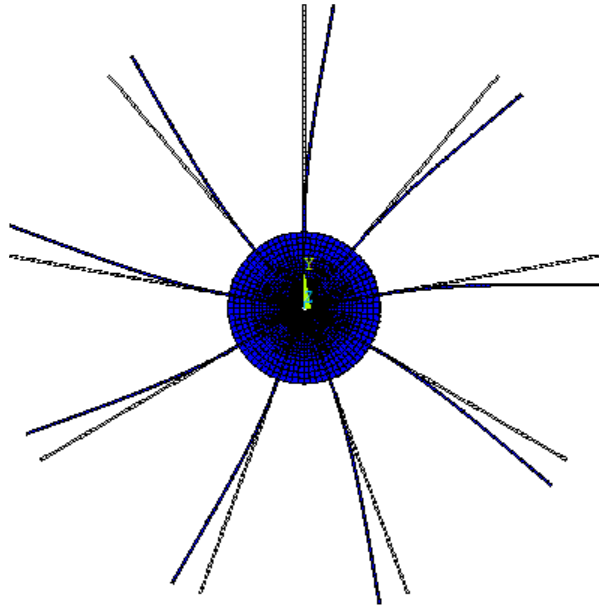


Figure 22: Zero nodal diameter mode shape

It is evident both from fig. 21 and 22 that the displacement of the blades is the same in the same direction as predicted.

4.2 Bladed Rotor modelling

Differently from the other rotors of the previous chapters, for this model, just solid elements (SOLID 186) have been used in order to discretize the structure. The mesh in particular is obtained by replicating one meshed sector (like in fig. 13) of the assembly Blisc-shaft. In this way it is possible to obtain a discretization which is as homogeneous as possible, avoiding the risk of having variations in stiffness and mass distribution due to difference in the mesh. Moreover, as announces the title of the chapter, the scheme of the constraints and of the model is the same of the simple Stodola-Green rotor model: this time there is just a difference for what concerns the dimensions which have been increased (Drawing in the APPENDIX). Using these dimensions it is possible to obtain numbers, at 0 rpm, comparable with the base Stodola-Green model. On the other hand such a bigger bladed disc, compared to the shaft, allows a clear identification of the mode shapes (fig. 23). Anyway, the first part of the process has been dedicated to the understanding of the results. For this purpose a geometry analogous to the one of [1] was employed (drawing in the appendix).

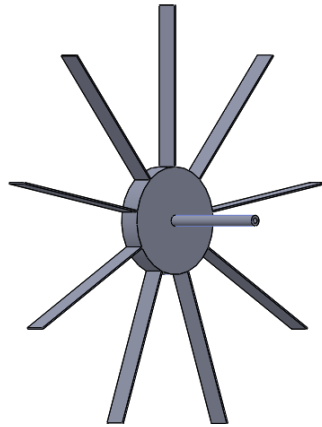


Figure 23: Bladed Stodola-Green rotor with 90° pitch angle

4.3 Model validation

The first step of the process concerns the validation of the mathematical model replicating the results of the article [1]. This step is fundamental in order to understand precisely what happens in the analysis. Having this article as term of comparison helped a lot since the the main struggles were about the use of the software and the identification of the different modal families.

4.3.1 Solver peculiarities

Another fundamental step is the identification of the commands to supply to the software to obtain a pre-stressed analysis of an asymmetric rotor: in fact, as all the bladed disc built by identical circular sectors (such as turbine discs, propellers etc.), this rotor is *NOT* symmetric. This detail is important because, the software requires the use of the *rotating reference frame* for the solution. So, in this way, the imaginary part of the eigenvalue represents the frequency in the rotating reference frame. For this model, and the following, also the centrifugal stiffening has been added from the beginning because for the slenderness of the blades it is possible to have an important effect on the frequencies given by this particular, as seen in the theory part.

4.3.2 Dynamic behaviour of the blisc-shaft assembly with pitch angle of 90°

As the previous chapter shows, in order to access the dynamic behavior of the model in the free response configuration, a Campbell diagram was plotted. The computations have been extended on the first 10 complex frequencies since, usually, the lowest frequencies are the ones which cause more problems, in terms of amplitude of displacements, when excited. In fig.24 is possible to appreciate the mentioned Campbell diagram in the rotating reference frame. The denomination of the data in the legend is made accordingly to the stationary reference frame for simplicity:

- the curve called 'Shaft FW', decreasing and increasing, (fig.24) represents what in the stationary reference frame is the forward whirl motion and, consists in a flexural excitation of the shaft (fig.25);
- the orange curve (fig.24), 'Shaft BW + Nd1 BW', begins in the same point as the 'Shaft FW' and then disappear under the frequencies denominated 'Nd.'. This is emblematic

of a particular feature of this family of frequencies which begins as a shaft modal shape (fig.25) and becomes a blade-shaft mixed one (fig.25);

- the rest of the data (denominated 'Nd..BW/FW') plotted ,superposed to the 'Shaft BW + Nd1 BW' curve (fig.24), show in principle modes of blade. In fact, since the disc is really rigid with respect to the blades, what is going to vibrate is just the blade (fig.25), as seen in the previous section.
- the curves denominated as 'Nd1 FW + Shaft FW' and 'Nd1 BW + Shaft BW' are the two families of frequencies starting as modes of blade and becoming a mix between shaft and blade modes after the veering process with the 'Shaft BW + Nd1 BW' curve;
- the frequencies denominated 'Nd0' represent a mode shape which does not vary a lot with the rotational speed, and couples zero diameter vibration with the torsional vibration of the shaft.

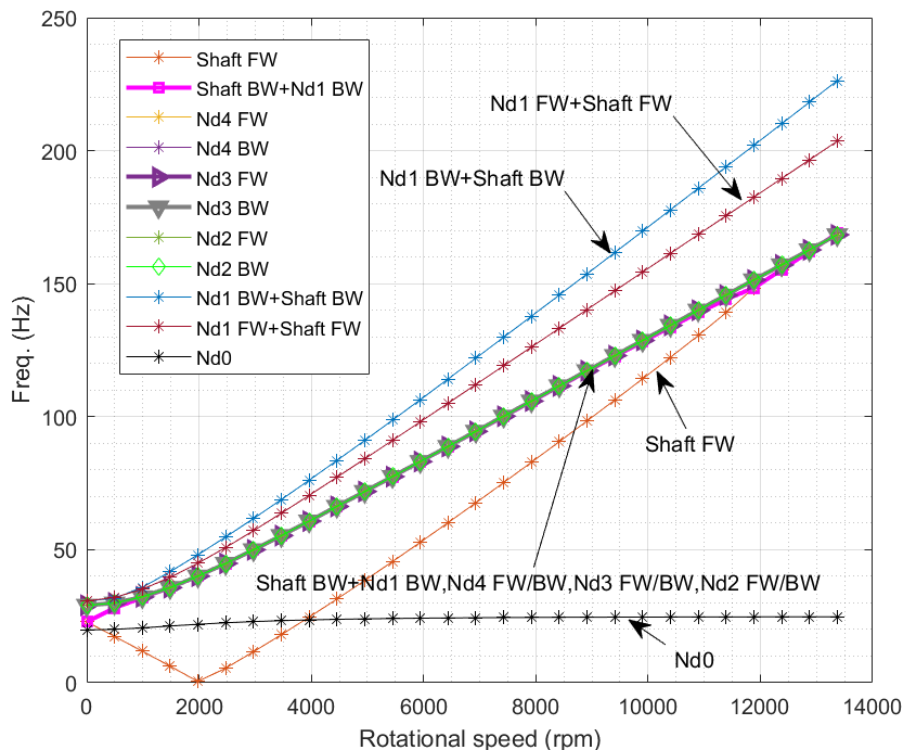


Figure 24: Campbell Diagram in the rotating reference frame of Bladed Stodola-Green rotor with 90° pitch angle

After this rough description of the results of the model, it is good to point out the peculiarities:

- the first evident feature is the drop to zero of the 'Shaft FW' frequency. This is particularly helpful since allows us to identify immediately the the critical speed: in fact since in the rotational reference frame, that curve is obtained subtracting the rotational speed to the frequency, when the two values are equal, the critical speed is spot;
- between 'Shaft FW' and the 'Shaft BW + Nd1 BW' it is possible to notice a frequency split to be imputed to the gyroscopic effect;

- there is an exchange of modes (at about 500 rpm), called '*veering*' in literature, between the 'Shaft BW + Nd1 BW' curve and the ones denominated 'Nd1 FW + Shaft FW' and 'Nd1 BW + Shaft BW': this veering phenomenon turns the 'Shaft BW + Nd1 BW' family in a blade mode and the other 2 families in a mix of shaft and blade mode;
- at around 12000 rpm the 'Shaft BW + Nd1 BW' curve returns into a pure shaft mode meeting the 'Shaft FW' curve;
- in the curves denominated 'Nd1 BW/FW + Shaft BW/FW' is possible to notice a split to which they undergone. This split is given by the blades exerting a bending excitation on the spin axis which [1], which with the help of the Gyroscopic effect, determines their frequency split;

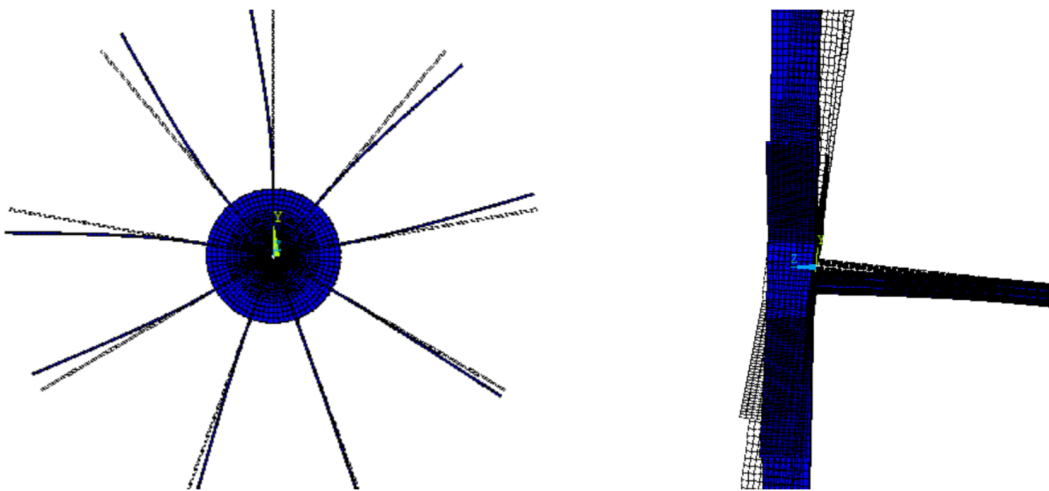


Figure 25: Respectively flexural shaft mode on the right and blade flexural in plane mode on the left, where the blue profile represents the undeformed configuration

Another predictable behaviour of the system is related to the rise of the blade modes (denominated in fig. 24 '*Nd..BW/FW*') which are, in a certain way, expected since the system is constituted by a really compliant shaft and a really stiff disc. This gives birth to the classical modes describing the behaviour of the bladed discs:

- in particular 8 modes of blade are present, which represent the 4 nodal diameters (non counting the zero nodal diameter) of which the bladed disc disposes;
- these modes are 8 (not counting the zero nodal diameter mode) since they are couples of the same mode, one rotating clockwise and the other counterclockwise on the bladed disc;
- their frequencies are really close to each other (they all start at 29 Hz as possible to see also in the first modal family in fig. 19 and go on at the same frequencies fig. 24) and in the representation in fig. 24 they result as superposed.

In order to understand that those frequencies, which differs of some tenths of Hz, belonged to the different modal diameters, it was necessary to plot the displacement of the tips versus the number of the sector, for what concerns the data coming from the rotordynamic analysis

and, compare them to the ones coming from the modal analysis of the bladed disc (fig. 26). The curves of the modal analysis are not always the same (in fig. 26) since some of the curves of fig. 19 have been translated of some sectors: anyway this is a regular operation since the modes are harmonic and rotating on the structure.

Another feature of these frequencies to note is that their increasing behaviour is mostly due, as shown in eq. 21 (eq.13.71 of [3]), to the rotational speed. The fact that the blade frequency increases monotonically with the rotational speed [5] is an effect related to the centrifugal stiffening. In fact neglecting this last one, the curve of these frequencies would come out flat as the speed increases.

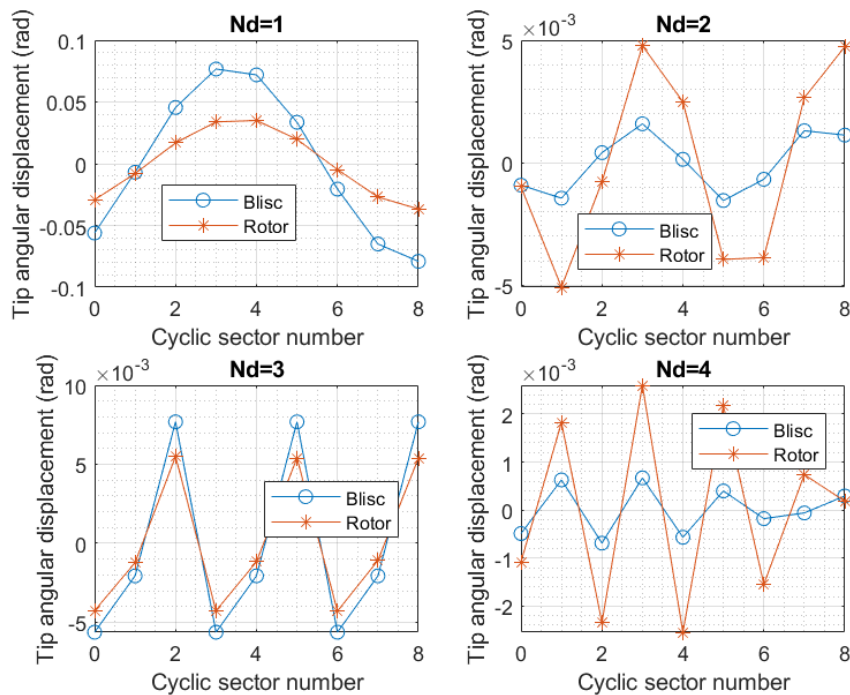


Figure 26: Angular tip displacement comparison in order to identify the identity of the modes extracted in the rotor analysis (at 29 Hz) with respect to the ones found in the modal analysis of the bladed disc

Last but not least there is an instability phenomenon which verifies at around 12000 rpm and is predictable since of the ratio between the radius of the disc and the blade length is less than one (from the theory of the rotating pendulum in [3]). This instability is connected to the 'Shaft FW' frequencies. No evidences of this fact are present in the Campbell diagram since the phenomenon is recognizable from the real part of the eigenvalue (Laplace) turning positive. At the end, it is good, to have clearer in mind what happens from our physical point of view, the Campbell diagram in the non rotating reference frame was plotted (fig.27). This is done by subtracting or adding the rotational speed to the frequency found in the non-inertial reference frame. In conclusion in this diagram it is possible to notice the stiffening phenomenon, represented by the the frequency split, due to the gyroscopic effect mainly on the bending modes of shaft (since the others 'stiffening' are due to the centrifugal field). A peculiarity to underline is the change in direction of rotation of the 'Shaft BW + Nd1 BW' mode and the other modes of blades. This fact is represented by the rising branch after the meeting with the x axis (effect given by the

centrifugal stiffening phenomenon without which the frequencies would just tend to zero as ω increases) and, was already encountered for the 'Shaft FW' curve in the rotating reference frame.

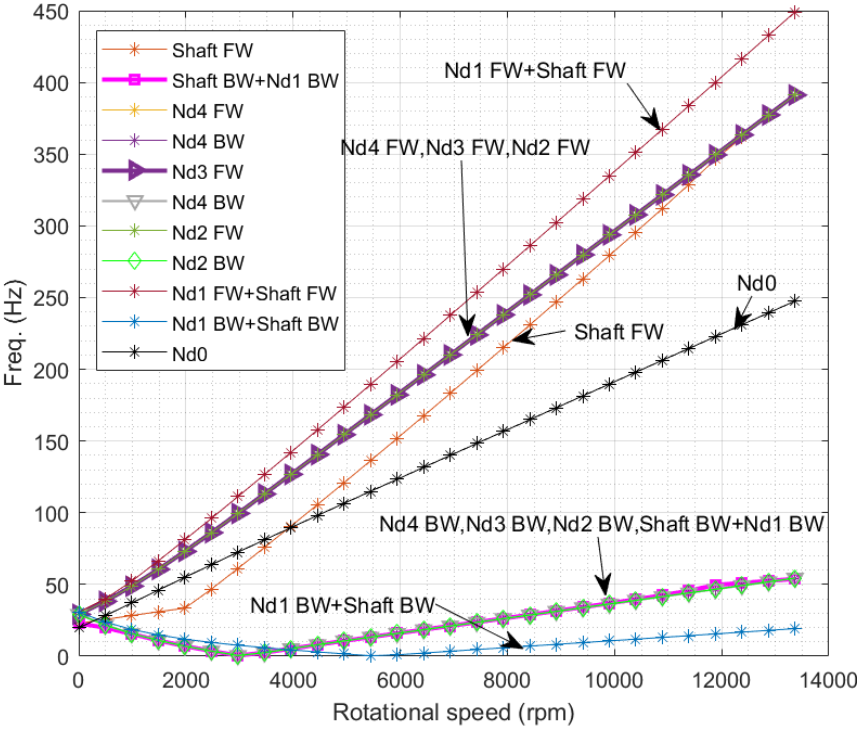


Figure 27: Campbell diagram in the inertial reference frame

4.4 Evaluation of the influence of the blade pitch angle on the dynamic behaviour

The evaluation of the change of frequency given by the the change of the pitch angle of the blade is fundamental. In fact, for example there are some planes like the ATR-72 for which the pitch angle of the propeller is variable due to efficiency reasons. What has been done in this case is studying the change in frequency with reference to the ones in the rotating reference frame including, as before, the gyroscopic effect. From the theory of the rotating pendulum it is expected a change in the frequency due to the change of the pitch angle. The purpose here is to assess the effect on the assembly dynamic behaviour.

4.4.1 Description of the model

Compared to previous blisc-shaft assembly, for the extraction of these results the disc had to be modified at the blade base in order to have the same blade disc attach for all the different cases (fig.28). This allows not to have influences of the different masses and stiffness that would come out if just the blade pitch angle was changed maintaining the curvature of the disc (drawing in the appendix). Moreover, the mesh this time implies, since of the impossibility of obtaining a mapped mesh with brick elements, tetrahedonal elements (10 nodes) for the 'disc' volume. These elements are anyway a variation of the brick element SOLID 186. The constraints as always are put in order to simulate a cantilever at the free end of the shaft.

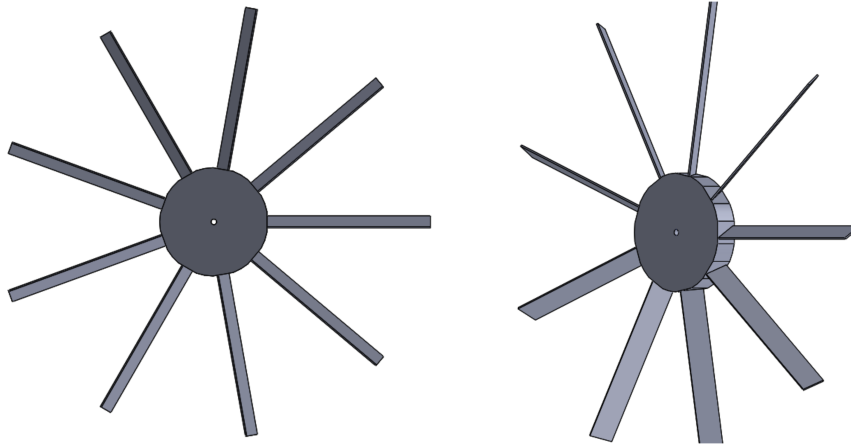


Figure 28: Modified bladed disc with pitch angle of the blades of 60°

4.4.2 Comparison of the different pitched assemblies behaviour

The results obtained for this calculation allow us to plot the Campbell diagram of each version of the model. In particular fig.29 holds the same notation as the previous diagrams or, in other words, the legend related to the inertial reference frame.

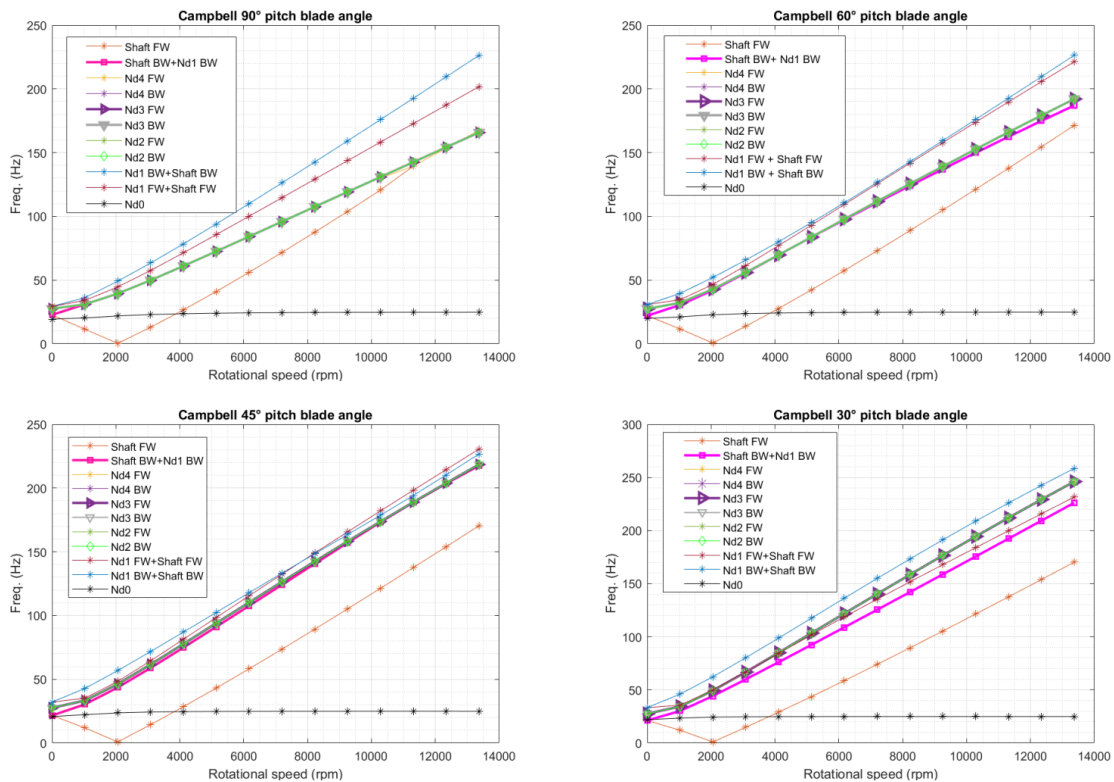


Figure 29: Campbell diagram changing the pitch angle

At first sight comes to the eyes the fact that, as the pitch angle decreases, there is no more

convergence of the 'Shaft BW + Nd1 BW' and 'Shaft FW' curves which tend to diverge. This thus leads to an increase in the frequency as shown in fig. 30.

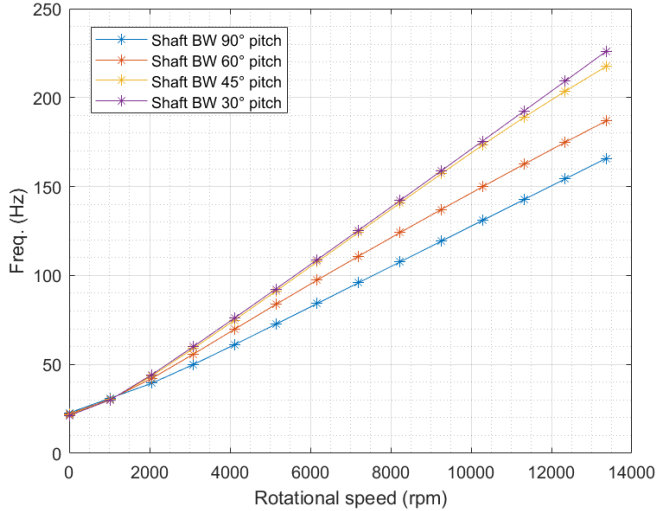


Figure 30: Backward whirl frequencies comparison as the pitch angle changes

Another peculiar feature of the 'Shaft BW + Nd1 BW' modal family is that, as anyone logically can predict, more the curve differentiate from the 'Nd..BW/FW' curves, more the influence of the bending mode shape rises, up to the 30° pitch angle 'Shaft BW + Nd1 BW' curve, whose behaviour is mainly flexural as the 'Shaft FW' one. This could be explained because the excitation of the blades on the shaft, coupled with the gyroscopic effect, is higher in the case of the 30° pitch angle: the cause can be imputed to the fact that the mode shape resulting from the vibration of the blades, in this case, is no more representing an in plane motion but an out of plane one (fig. 31).

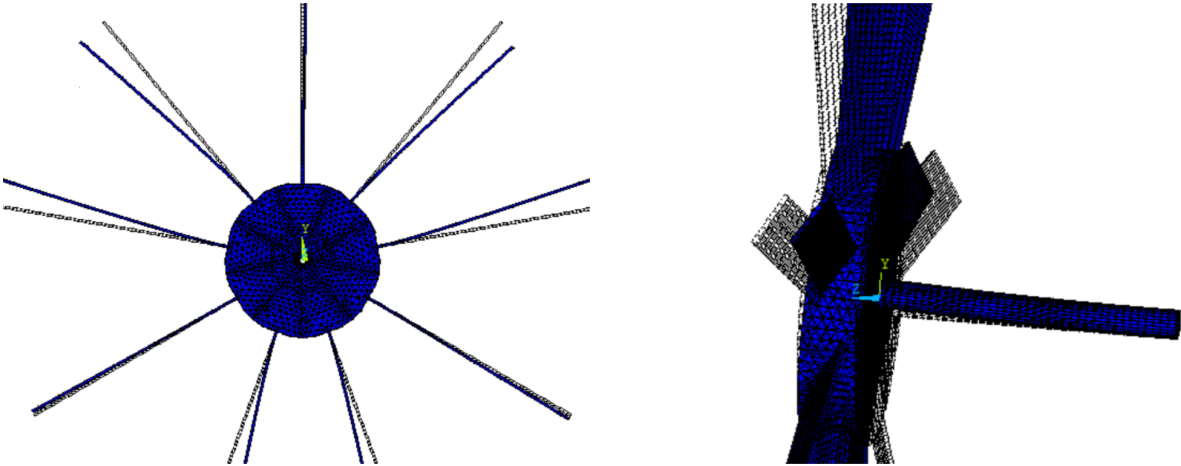


Figure 31: Respectively pure in plane blade vibration (90° pitch, on the left) and predominant bending mode (30° pitch, on the right) at the same rotational speed of 7198 rpm for the 'Shaft BW + Nd1 BW' curve

On the contrary, as predictable, the difference between the 'Shaft FW' curves is minimal (fig. 32). This is understandable since, being this a bending mode of the shaft, the blades are not implied actively in the vibration and do not exert any vibrational contribution.

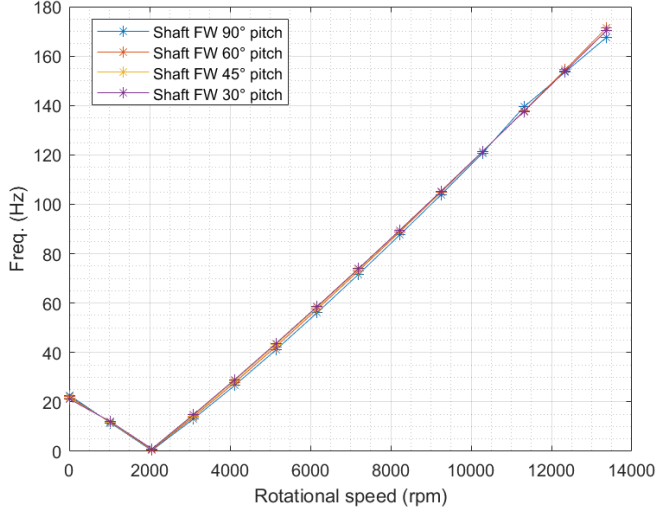


Figure 32: Forward whirl frequencies comparison as the pitch angle changes

Stating this behaviour for the 'Shaft FW' mode, it is possible also to declare that the small difference found on these frequencies is imputable to the gyroscopic effect on the assembly, since the centrifugal stiffening and the spin softening act in the same way since the main vibrating part is the shaft. In order to quantify the outcoming frequency difference, a graph (fig. 33) has been prepared.

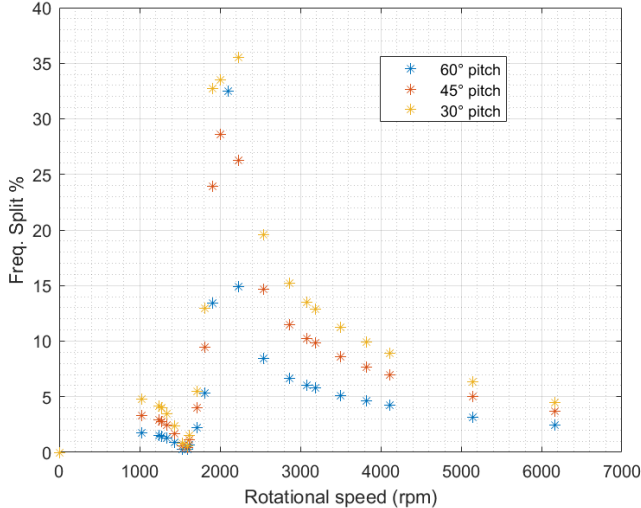


Figure 33: Frequency split in absolute value with respect to the 90° pitch angle case for the 'Shaft FW' mode

From this graph is possible to conclude that the highest frequency split with respect to the 90°

case is found, another time, decreasing the pitch angle (fig. 33). On the other hand, once the vibration of the blades comes into play, the frequency difference becomes higher but, this time, is imputable to the pitch angle itself as shown in 20 (fig. 34).

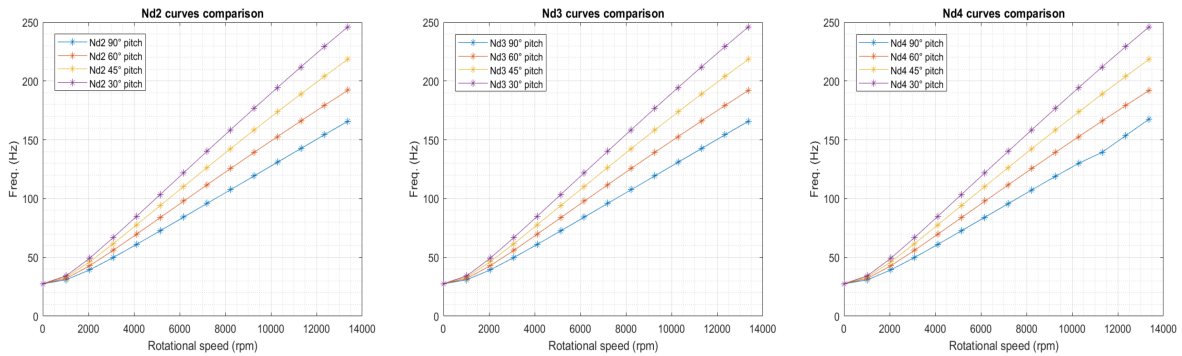


Figure 34: Blade modes curves comparison

As it is possible to observe from fig. 34, since the curves describing the nodal diameter 2 up to the nodal diameter 4 are almost superposed in all the cases, the split among their frequencies is the same up to a maximum value of 80 Hz at around 14000 rpm. If compared to these splits, the frequencies splits due to the families characterized by a nodal diameter equal to one are lower. This happens, as before, since the curves in fig. 35 describe mixed modal shapes between blades ones and shaft ones (bending modes of shaft).

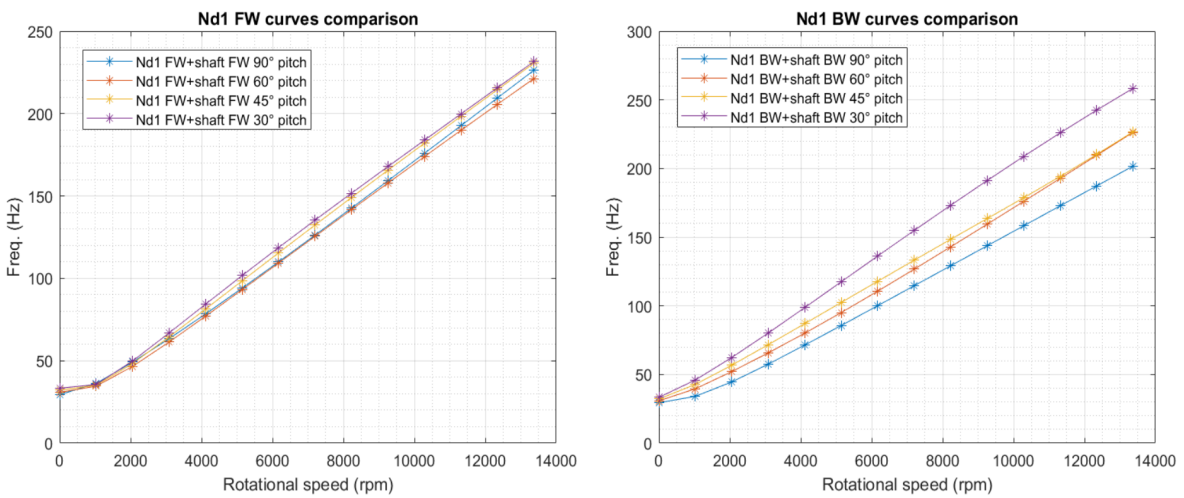


Figure 35: One nodal diameter curves comparison

In fact the maximum splits in fig. 35 are respectively 10 and 57 Hz at 14000 rpm.

For what concerns, instead, the vibration given by the 'Nd0' curve, which couples the zero nodal diameter and the shaft torsional vibration, the frequencies start as different of some Hz and then converge as the rotational speed increases (fig. 36).

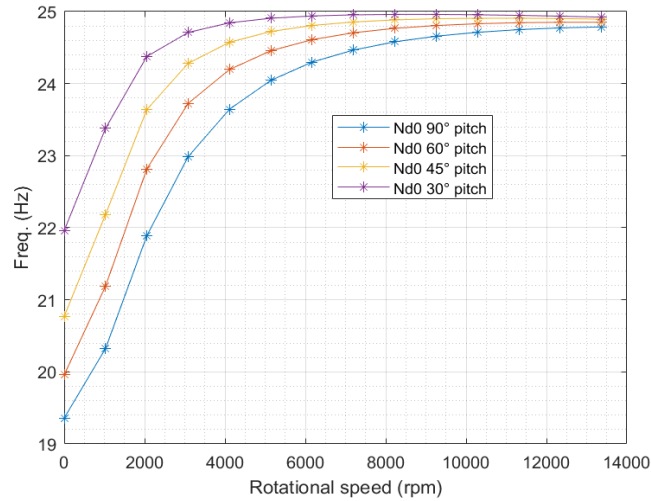


Figure 36: Zero nodal diameter curves comparison

The frequency difference at 0 rpm can be due to the fact that the vibration of the blades changes progressively from an in plane one, exciting mainly the torsional behaviour of the shaft, to an out of plane one coupled with the axial behaviour of the shaft. Moreover, at high speed the frequencies converge, since the stiffening effect inhibits the blade vibrations and turns all mode shapes into a pure torsional shaft mode.

Last but not least, it is important to underline that the instability (rising at 12000 rpm), due to the ratio between radius and blade length being less than one, disappears changing the value of the pitch angle from 90° (instability related to the 'FW' mode). This was expected from the theory of the rotating blade constrained to oscillate in a plane [3].

5 Modelling of the propeller shaft assembly of the engine of the ATR-72

5.1 General overview of the ATR72

The ATR-72 is a short haul plane (1100-1500 km) powered by a twin turboprop engine. It is principally a Civil plane even though it has some military versions. As the name predicts, its passenger carrying configuration could seat 72 to 78 people in a single class arrangement. The current production series is the ATR72-600 which is different, from the previous ones, since a lot of structural parts have been substituted in order to make the structure lighter and, in this way, increase the performances and the efficiency.

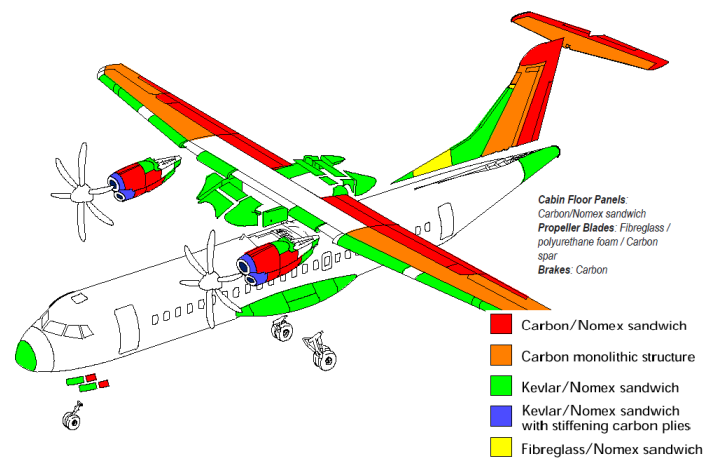


Figure 37: Use of composite materials in the ATR72 structure

5.2 General overview of open rotors technology

Open rotors technology is not a new engineering discover but has been used since the past in the aviation field for the propulsion of planes. Since the 2nd World War with the wide development and spread of the jet and turbojet engines, the upper mentioned architecture has been stopped in its diffusion and innovation. In recent times the open rotor solution has come back into the field for advantages in efficiency problems.

5.3 Propeller model

In order to evaluate the influences of the gyroscopic effect on the ATR-72 propeller, the work has started from the creation of a 3D-model. It is important to underline that, since the precise data for the geometries and the materials are not available for industrial purposes, they are obtained starting from images and some drawings found online. The model (fig. 38) schematize the structures and the masses directly connected to the blades and to the rotor shaft.

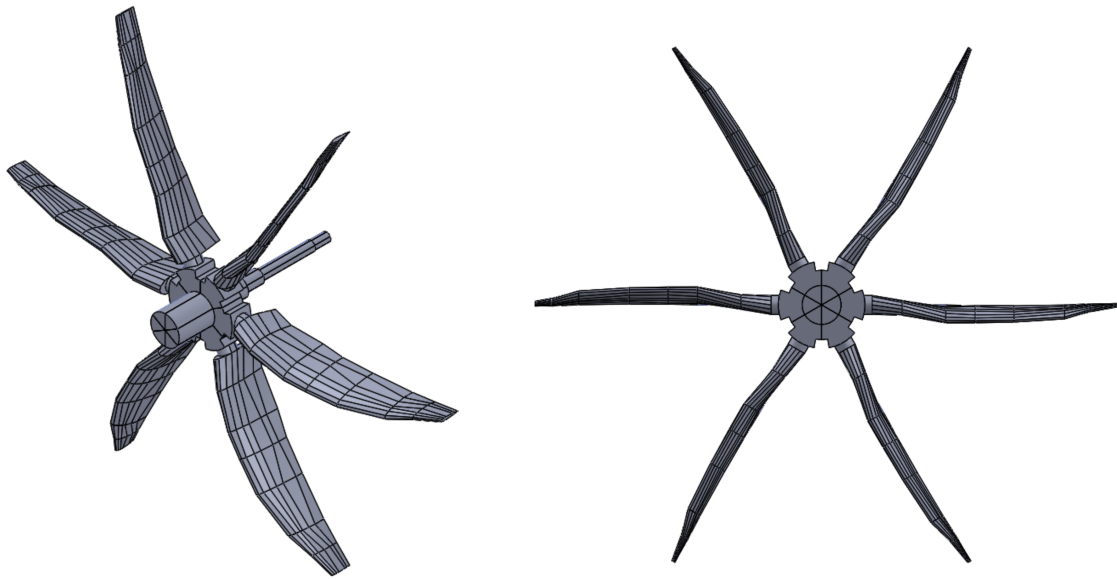


Figure 38: Simplified model used to represent the shaft and propeller assembly of the ATR-72

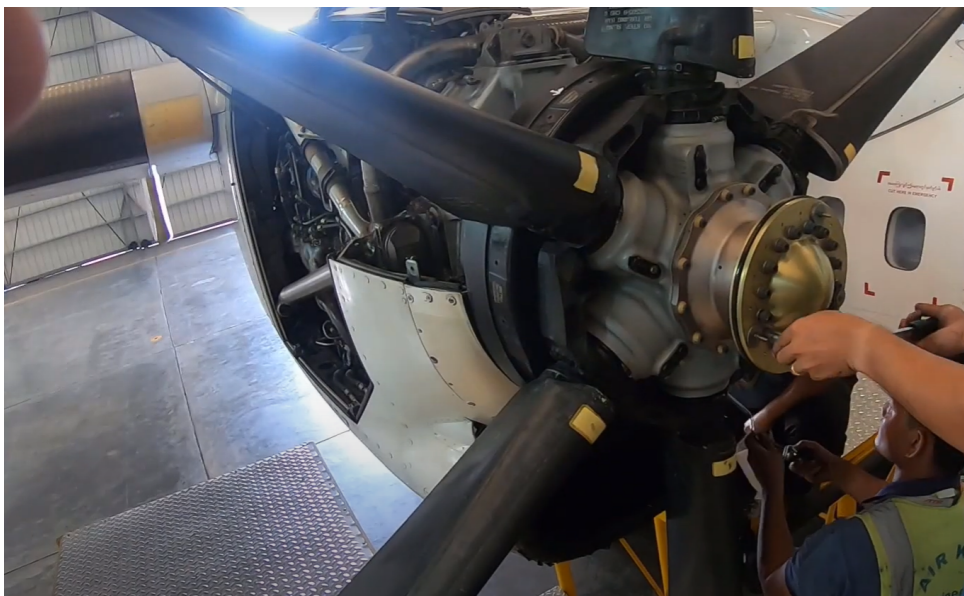


Figure 39: Real picture of the ATR72 modelled part

A particular attention has been put on the drawing of the blade which is tilted along its length. In fact the challenge was constituted not only from the drawing itself and from the lack of informations about the dimensions but also, from the fact that a model with a reasonable quantity of nodes in the FE analysis was needed. In other words the model had to be run on a not so powerful hardware (laptop). So the main concern was about the drawing of the blade which has been obtained, at the end, by a simplification which consisted in the substitution of the continuous line, along the length of the profile, with some small straight segments (fig. 40). This holds also for what concerns the drawing of the wing profile: for this purpose, some points of a

	Composite material	Steel
Density (kg/m ³)	800	7800
Elastic modulus (MPa)	41778	210000

Table 1: Materials properties

NACA4 curve were calculated and used in order to draw the lines useful for approximating the profile (fig.40).

5.3.1 Material choice

Another issue was constituted by the choice of the materials: for what concerns the disc constraining the blades, the cylinder attached to it and the shaft, they were assumed to be made of steel. For the blade, instead, the process was more complicated since from the description of the propfan engine, it is known that they are made of composite material. In particular, to guarantee the lightweight and the proper mechanical properties, the blade is made as a sandwich structure: the outer skin in fact is made of carbon fiber and the inner core is filled with a foam. This informations were acquired not directly from a single source but from the comparison of multiple sources on the subject of the lightweight blades mounted on modern airplanes. At the end the choice of the material for the blades has fallen on a compromise which took into account the problem, sticking to reality but also simplifying it: the blade has been built with isotropic elastic properties and as elastic modulus the value found in the article [6]. This value has been obtained trough an experimental 3 point bending test, considering a sandwich panel constituted by a carbon skin of 8 layers and a poliurethane foam core (tab. 1). The value of the elastic modulus chosen is taken from a bending test since the behavior of the blade is mainly flexural in plane (for the configuration chosen in fig. 38). Moreover, the equivalent density has been evaluated taking into account the values of the single materials and the dimension of the part.

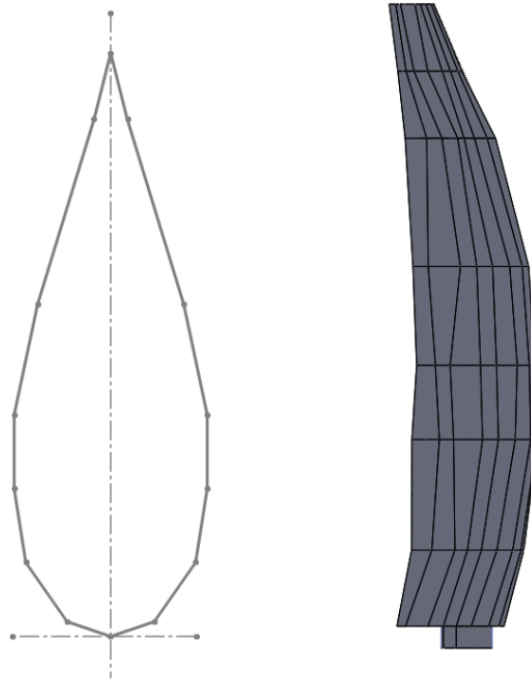


Figure 40: On the left the NACA4 discretized profile, on the right the simplified blade drawing

5.3.2 Constraints setting

As already said the drawings of the assembly parts are obtained by non official technical drawings so, also the choice of the dimensions of the shaft is reasonable but, probably, does not comply to the real part. Moreover, also the casing and the bearings mounted are unknown: what it is assumable is their position based on how the shaft was modeled. Obviously then, they for sure will constrain both the radial and axial displacement. The locking of the last degree of freedom is fundamental, as seen before, since an axial thrust coming from the dynamic vibrations, will be always present as the pitch angle becomes lower than 90° and the blade modes turn into out of plane modes (the ATR-72 has the possibility of varying the pitch angle). In the end the constraints settings is composed by one hinge and a simple support (in all the directions) as shown in fig. 41.

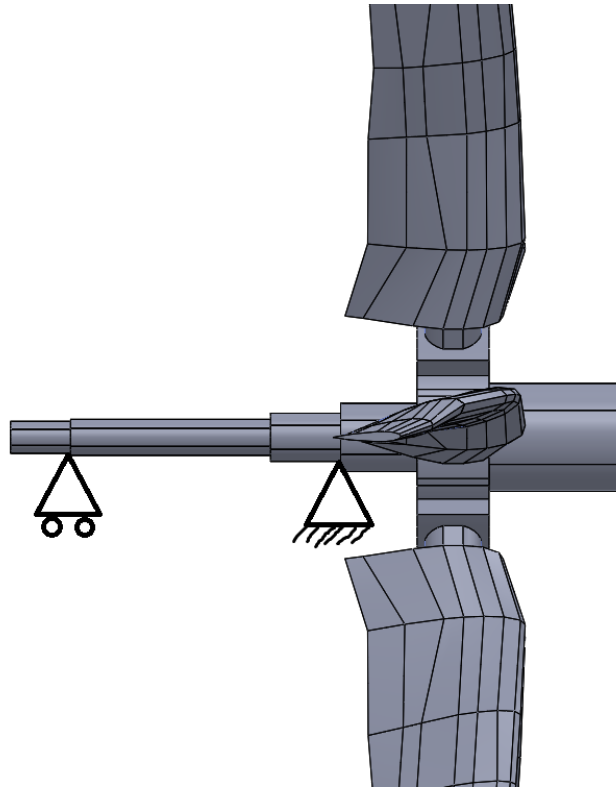


Figure 41: Model constraints

5.4 Dynamic behaviour of the ATR-72 assembly

As before, in order to assess the dynamic behaviour of the assembly composed by the Propeller of the ATR-72 and its shaft, a Campbell diagram of the structure has been plotted. Taking into account that the pitch angle of the blade varies along its height, the case studied was that taking as reference the first pitch angle of the NACA4 profile (the first one starting from the blade attach) as a 90° angle. The choice of studying this case only has turned out successful since the behaviour of the 'blisc' is more or less the same as the one studied in the previous chapter. In fact, another time, the bulky profile of what it is possible to call approximately as disk (but really is constituted by the blades attach and a cylindrical disc) does not contribute to the mode shapes of the propeller assembly. So in other words a good approximation in this case is constituted by a rigid disk where only blade modes are present. So, as already said, the behavior of the assembly propeller-shaft is the same as the model analysed in the previous chapter. Referring to the rotating reference system, the Campbell diagram has been obtained for a speed range comprised between 0 and 14000 rpm (fig. 42):

- it is possible to notice as before the 'Shaft FW' curve whose name is another time referred for convention to the inertial reference frame (fig. 42) and still represents a flexural mode of shaft;
- as the previous chapter also the 'Shaft BW + Nd1 BW' represents a flexural shaft mode at the beginning and then turns into a blade mode;
- the families of frequencies representing the modes of blade (denominated as 'Nd..FW/BW') from the nodal diameter equal to 2 to the nodal diameter equal to 3 are superposed;

- the curves referred to the the modes starting as blade mode with nodal diameter equal to one and becoming a mix between a blade and a shaft mode are highlighted as 'Nd1 BW+Shaft BW', 'Nd1 FW+Shaft FW';
- The curve curve denominated 'Nd0' is related to a mode of blade and in particular to the nodal diameter zero.

After listing all the modes it is dutiful to describe in deep what happens to the system in this range of speeds:

- the 'shaft FW', curve as before, tells us where it is situated the critical speed (around 5200 rpm). The mode shape is a bending mode of shaft and changes the direction of rotation after the critical speed (due to centrifugal stiffening phenomenon);
- the 'Shaft BW + Nd1 BW' family represents at the beginning a flexural mode of shaft but at around 2000 rpm there is a veering phenomenon ,interesting this mode and 'Nd1 FW + Shaft FW /Nd1 BW + Shaft BW' , which transforms the behaviour of the mode into a blade mode with nodal diameter equal to one (and in this way become superposed by the other blade modes);
- the curves denominated 'Nd1 BW+Shaft BW', 'Nd1 FW+Shaft FW' show, after the 2000 rpm, a behaviour characterized by a flexural excitation of the shaft and, before the 2000 rpm, a pure blade flexural mode characterized by one nodal diameter;
- For the blade modes (denominated ad 'Nd..'), their shape is found to be, for the majority, the one of an in plane vibration : this is due for sure to the pitch angle with respect to the first section of the blade and the fact that in the lower part the blade is thicker.

A particular feature is constituted by the fact that, since the the number of cyclic sector of the propeller can be thought to be coincident with 6, since of the 6 blades, the eigenvalues coming from the solution of the modal analysis are always complex with multiplicity 2 except for 2 cases: the case of the nodal diameter zero and the case of the nodal diameter 3. In fact, if in the first scenario the blades are vibrating in phase, in the other one they are rotating in anti-phase or mathematically with a phase angle of pi. It is important to remark that this last condition is possible just if an even number of cyclic sectors is present, if not, like in the case of the previous chapter, only the nodal diameter equal to zero has a real solution.

As in the previous chapter , the 'Nd0' family exhibits an in plane vibration coupled with the torsional motion of the shaft.

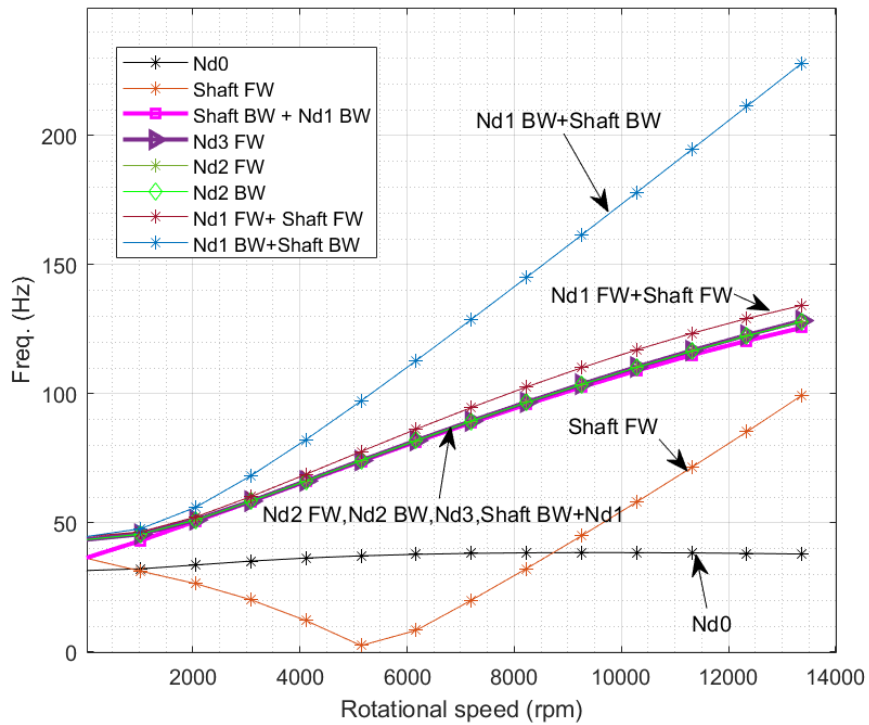


Figure 42: Campbell diagram of the ATR-72 propeller model in the rotating reference frame

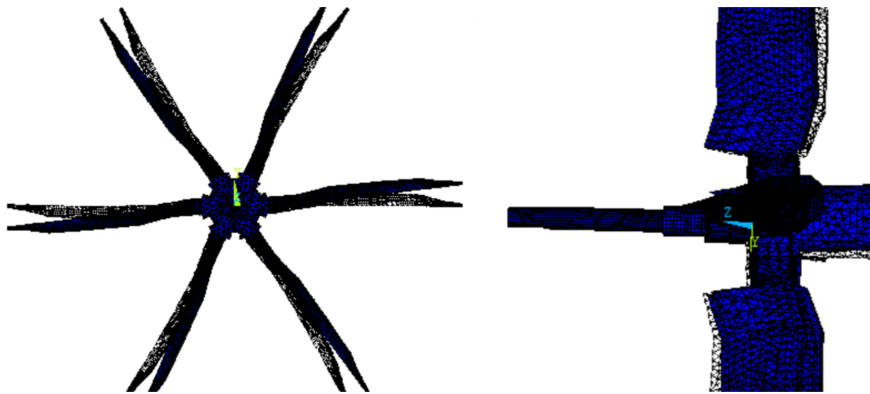


Figure 43: Respectively blade mode corresponding to nodal diameter equal to zero and bending mode of shaft

At this point, in order to stick to the reality, it is necessary to point out a consideration concerning the maximum rotational speed reached by the propeller: in fact as declared by the manufacturer on its website the propeller of the PW120 (model of the turboprop engine by Pratt and Withney) spins at a maximum rotational speed of 1200 rpm. So what has to be done is evaluating the behaviour of our system in the restricted range (fig. 44).

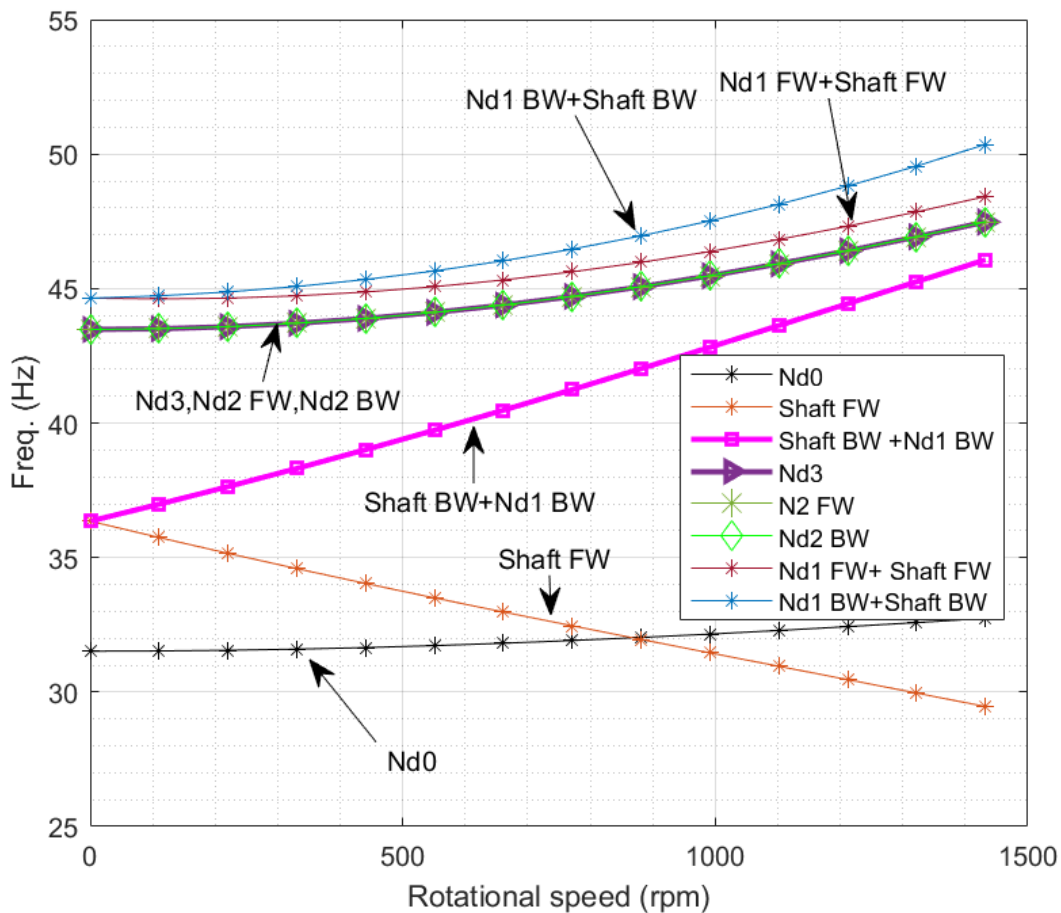


Figure 44: Campbell diagram of the ATR-72 propeller model in the rotating reference frame in the restricted range

The curves trend, as before, is the same as the one seen in the previous picture (fig. 42). The main features in (fig. 44) concern the influence of the gyroscopic effect on the frequencies:

- it is possible to observe the frequency split between 'Shaft BW + Nd1 BW' and the 'Shaft FW' curve given by the gyroscopic effect;
- the gyroscopic effect influence is visible another time for 'Nd1 BW + Shaft BW', 'Nd1 FW + Shaft FW' for which anyway, the effect is attenuated since the mode has a predominance of the blade vibrating effect up to 2000 rpm;

In conclusion what is really important to underline, is the fact that in the range analysed there are two missing factors who are usually not good to find in the working range: the critical speed and the instability field. For what concerns the instability, this value, for a system similar to this, comes out at high rotational speeds as seen in the previous chapter. So, its calculation turns out to be more an exercise than a practical need. If the model was precise it would be possible to say the same also for the critical speed: since the model is an approximation what is possible to say is that engineers, most likely, tuned the system in such a way not to encounter the critical speed value. The last particular to be nominated is the fact that, it is true, as previously said, that the frequencies of blade are for the most described by an in plane vibration but, since of the change

of the pitch angle along the height of the blade, there is always a light coupling with the axial vibration.

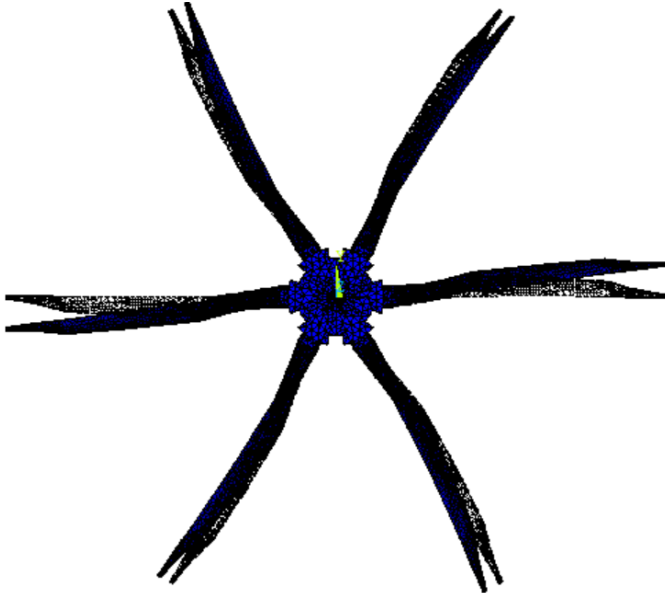


Figure 45: Front view of the blade mode corresponding to the nodal diameter equal to 2

6 Conclusion

At the end it what is worth to say in order to make a summary of this work in the following: when analyzing a bladed disk-shaft assembly, it will be always possible to find some common features in the behaviour. One of this feature is always constituted by the particular way of vibrating of the bladed disk. Its behaviour will be always characterized by mode shapes associated to the nodal diameters. Moreover, considering a propeller-shaft assembly of the open rotor of a plane, probably, since the the part where the blades are connected to the shaft has not to be compliant at all, it will be bulky and whereby the most evident mode shapes will be the ones of the blades. On the other hand, considering the right supports such as bearings and casings, it is possible to avoid to strong excitation of the shaft which could lead to the instability of the system, at least for what concerns a reasonable range of speed: for reasonable in fact it is intended a range in which commonly a propeller does work (not like a range of 0-14000rpm). In fact as seen in the chapter 5, the speed range of rotation of a real propeller, used in a turboprop engine, is between 0 and 1000 rpm. Also the critical speed is a property which has to be assessed and tuned in advance. In conclusion, all these computations represent a good starting point to understand the peculiarities of the behaviour of a propeller-shaft assembly. Anyway it has to be considered that, a forced analysis should be performed to effectively asses which of the excitation can be possibly constitute a danger for the structural integrity of the engine during its life. Such an analysis would include also the determination of the characteristics of the damping of the bearings and of the materials, the excitation coming from the engine and from the aerodynamic interactions. For example, the damping related to the bearings would constitute a light factor of variation for what concerns also the whirling frequencies. At the end, each simulation of a real component must always be correlated to an experimental data acquisition in order to validate the model, which can not be always too much detailed for problems related to computational times, hardware and increasing time to market in general. It is anyway true that a good numerical model allows to avoid fatal dangerous behaviors of the part which can create a real loss of money after the piece has been brought to production.

For what concerns the numerical results obtained in the thesis we are pretty sure of the work done since we have successfully replicated the results obtained in [1] by our colleagues of the Imperial college (maybe with some small difference due to model slight changes), both for the case of the Stodola-Green (fig. 46) rotor and for the case of the Bladed Stodola Green rotor (fig. 47). About the last one, since our interest was all over the behaviour of the rotor, we took into consideration some more frequencies (like the one related to the nodal diameters different from one).

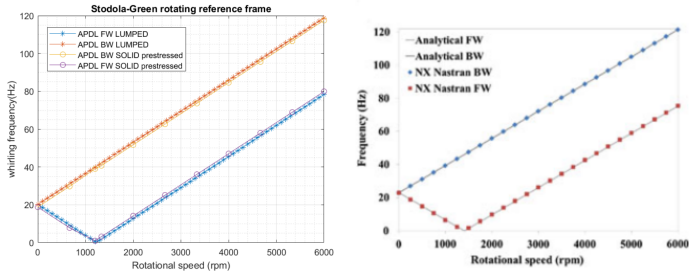


Figure 46: Stodola Green Campbell obtained in the thesis work and in [1]

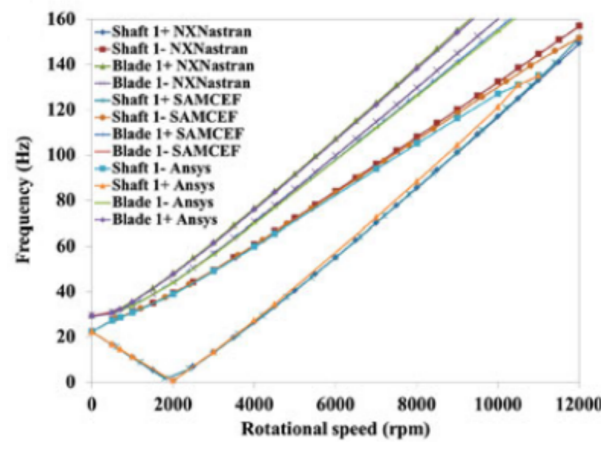
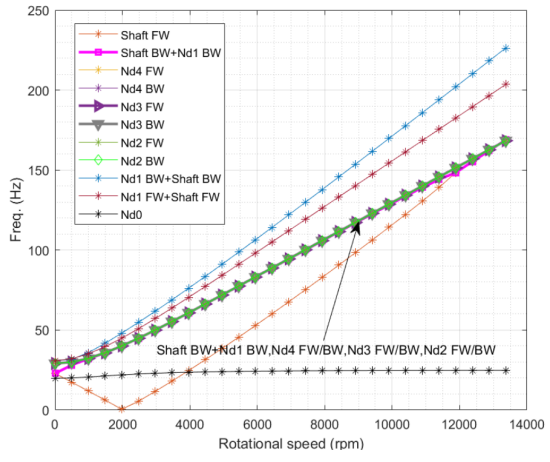


Figure 47: Bladed disk Campbell obtained in the thesis work and in [1]

7 Appendix

7.1 Ch.3

The following three pieces of code have to be used at the same time to perform the Stodola-Green free analysis. In order, they represent the main code for running the analysis and two functions. The first function serves as matrix assembler, while the second is used to decouple the equations and solve them separately.

7.1.1 Stodola-Green *Matlab* lumped model personally written

```
1 w=23*10^-3;      %disc thickness (m)
2 d=80*10^-3;      %disc diameter (m)
3 do=10*10^-3;     %(m) shaft outer diam.
4 di=7*10^-3;      %(m) shaft inner diam.
5 I=pi*do^4/64-pi*di^4/64; %(m^4) shaft mom. of Area
6 L=0.25;          %(m) shaft length
7 E=2.1*10^11;     %(N/m^2) Elastic modulus of the steel
8 Poiss=0.33;      %(-) Poisson ratio
9 G_el=E/2*((1+Poiss)); %(N/m^2) Shear elastic modulus
10 rho=7.8*10^3;   %(kg/m^3) Density of steel
11 V=w*pi*(d/2)^2; %(m^3) Volume of the disc
12 A_beam=pi*(do^2-di^2)/4; %(m^2) section of the beam
13 Vbeam=L*A_beam; %(m^3) volume of the beam
14 m=V*rho;        %disc mass(kg)
15 mbeam=Vbeam*rho;
16 Jt=(1/12)*m*(3*(d/2)^2+w^2); %(kg*m^2) disc transv. mom. of inertia
17 Jp=0.5*m*(d/2)^2; %(kg*m^2) disc polar mom. of inertia
18 OM=linspace(0,6000,1000); % rotational speed vector (rad/s)
19 n_el=2; %number of elements to discretize the beam
20 n_n=n_el+1; %number of nodes
21
22 %%MATRIX ASSEMBLY AND CONSTRAINTS APPLICATION
23
24 [K,M,G]=matrix_ass(L,rho,A_beam,E,I,m,n_el,Jt,Jp);
25
26 %constraints application (cantilever)
27 Kcons=K(3:length(K),3:length(K));
28 Mcons=M(3:length(M),3:length(M));
29 Gcons=G(3:length(G),3:length(G));
30
31 %SOLUTION
32 [om_sol,eigval]=diagSYS(OM,Mcons,Kcons,Gcons);
33
34 %Campbell diagram plot
35 figure()
36 for p=1:2*length(Mcons)
37 plot(OM,abs(imag(om_sol(:,p))));
38 hold on
39 end
40 grid on
41 title('Stodola-Green');
42 xlabel('Rotational speed (rad/s)');
43 ylabel('whirling frequency(rad/s)');
```

Listing 1: Stodola-Green lumped model Matlab Code

7.1.2 FUNCTION TO ASSEMBLE MATRICES

```

1
2
3 function [K,M,G]=matrix_ass(L,rho,A,E,Ix,m_disc,n_el,Jt,Jp)
4 n_n=n_el+1;
5
6 %beam stiffness matrix definition
7
8 [Kb]=(E*Ix/((L/n_el)^3))*[12,6*(L/n_el),-12,6*(L/n_el);...
9     6*(L/n_el),4*(L/n_el)^2,-6*(L/n_el),2*(L/n_el)^2;...
10    -12,-6*(L/n_el),12,-6*(L/n_el);...
11    6*(L/n_el),2*(L/n_el)^2,-6*(L/n_el),4*(L/n_el)^2];
12
13 %beam lumped mass matrix definition
14
15 [Mbd]=(rho*pi*A/4)*L/(n_el*2)*[1,((L/n_el)^2)/12,1,((L/n_el)^2)/12];
16 Mbd=diag(Mbd);
17
18 M=zeros(2*n_n);
19 K=zeros(2*n_n);
20
21 %Disc inertia properties definition
22 Mdisc=zeros(2*n_n,2*n_n);
23 Mdisc(2*n_n-1,2*n_n-1)=m_disc;
24 Mdisc(2*n_n,2*n_n)=Jt;
25
26 G=zeros(2*n_n,2*n_n);
27 G(2*n_n,2*n_n)=Jp;
28
29 for t=1:1:n_el
30 MM=zeros(2*n_n);
31 KK=zeros(2*n_n);
32 qq=2*(t-1)+1;           % counter
33 qq1=qq+3;               % counter
34
35 MM(qq:qq1,qq:qq1)=Mbd;
36 KK(qq:qq1,qq:qq1)=Kb;
37 M=M+MM;
38 K=K+KK;
39 end
40 M=M+Mdisc;

```

Listing 2: Stodola-Green lumped model assembly matrix function

7.1.3 FUNCTION TO DECOUPLE AND SOLVE THE SYSTEM

```

1
2 function [OMEGA,eival]=diagSYS(rot_speed,Mtot,Ktot,G)
3
4 %where md,kd,gd are the diagonals of the diagonalized matrices M,K,G
5
6 [OMEGA]=zeros(length(rot_speed),2*length(diag(Ktot)));
7
8 [eivect,eival]=eig(Ktot,Mtot);
9
10 %diagonalization of the matrices to decouple the equations
11

```

```

12 Kd=eivect'*Ktot*eivect;
13 Md=eivect'*Mtot*eivect;
14 Gd=eivect'*G*eivect;
15 kd=diag(Kd);
16 md=diag(Md);
17 gd=diag(Gd);
18
19 %eigenvalues extraction from the decoupled equations
20
21 for n=1:length(rot_speed)
22     for o=1:length(md)
23
24 coeff=[md(o),-1i*rot_speed(n)*gd(o),kd(o)];
25
26 OMEGA(n,2*o-1:2*o)=roots(coeff); %to find the whirling frequencies
27 %results are saved 2by2 in columns
28     end
29 end

```

Listing 3: Stodola-Green lumped model assembly matrix function

7.1.4 Stodola-Green Ansys APDL lumped model

Code to simulate a Stodola-Green rotor with lumped elements in *Ansys APDL*. The code uses just one element in order to simulate the shaft: obviously creating more nodes it is possible to change the discretization. Just copying the solution in the prompt bar in Ansys, the routine should work.

```

1
2 FINISH
3 /Clear,all
4 /prep7
5 /Title,Stodola-Green:Critical Speed/Campbell
6
7 !CONSTANTS DEFINITION
8 !Rotor properties
9 L=0.25      !shaft length
10 Di=0.007   !shaft inner diameter (m)
11 Ri=Di/2    !shaft inner radius (m)
12 Do=0.01    !shaft outer diameter (m)
13 Ro=Do/2    !shaft outer radius (m)
14 D=0.08     !disc diameter (m)
15 R=D/2      !disc radius (m)
16 w=0.023    !disc axial width (m)
17 $E=2.1E11$ !young modulus of steel (N/m^2)
18 PR=0.3     !Poisson ratio
19 Density=7800 ! (kg/m^3) density of steel
20 m=3.14*R**2*w*Density      !mass of the disc
21 Id=(m*((3*R**2)+(w**2)))/12 !mass moment of inertia around the
22     !axis different from the one of rotation (kg*m^2)
23 Ip=(m*R**2)/2      ! (kg*m^2) mass moment around the rotation axis
24
25 !DEFINING NUMBER OF BEAMS
26
27 !Speed characteristics
28
29 Start_rpm=0 !definition of the range of speed and of the increment
30 End_rpm=6000
31 Increment=100

```

```

32
33 !modal anlaysis prameters
34 N_modes=2 !number of modes to extract
35
36 !SHAFT ELEMENT
37 Et,1,beam188 !beam element selection
38 KEYOPT,1,3,2 !imposing to the element a quadratic shape function
39
40 !material properties
41 Mp,ex,1,E
42 Mp,prxy,1,PR
43 Mp,Dens,1,Density
44
45 !Section type of the shaft (circular)
46 Sectype,1,beam,ctube
47 Secdata,Ri,Ro,30 !data for the creation of the tubular section
48
49 !NODES CREATION
50 N,1,0
51 N,2,L
52
53 !Shaft element creation (in this case just
54 !one element to discretize the shaft)
55 Type,1
56 Mat,1
57 Secnum,1
58 E,1,2 !Assign the element to the nodes
59
60 !DISC-Concentrated mass
61 ET,2,Mass21 !element lumped mass selection
62 R,2,m,m,m,Ip,Id,Id
63 Type,2
64 Real,2
65 E,2 !location of lumped the mass on the shaft tip
66
67 !Boundary conditions (cantilever constraints)
68 /SOLU
69 D,1,uz
70 D,1,rotz
71 D,1,ux
72 D,1,rotz
73 D,1,uy
74 D,1,roty
75
76 ! solution TIME
77 /SOLU
78 Esel,s,ename,,188
79 Esel,a,ename,,21
80 Cm,rot_part,elem !creation of a group of elements in order
81 !to assign the rotational speed
82 Esel,all
83
84 !specify the rotational velocity of the rotating elements
85 !CHOICE OF QRDAMP eigensolver
86 Antype,modal
87 Modopt,qr damp,N_modes,,,on
88 Mxpand,N_modes
89 Coriolis,on,,,off !coriolis effect ON

```

```

90 !in the inertial reference frame (OFF)
91
92 !SOLUTION routine
93 *DO,J,Start_rpm,End_rpm,Increment
94 spinRPM=J
95 Spin_rds=spinRPM*6.28/60
96 Cmomega,rot_part, Spin_rds
97 !application of the rotational speed to
98 !the previous selected group (rot_part)
99 SOLVE
100 *ENDDO
101
102 /OUTPUT,Stodola_Green_RES,txt
103 FINISH
104 /post1
105 Set,list
106 Plcamp,0,1,rpm,0,rot_part,0
107 Prcamp,0,1,rpm,0,rot_part,0
108 FINISH

```

Listing 4: Stodola-Green lumped model assembly matrix function

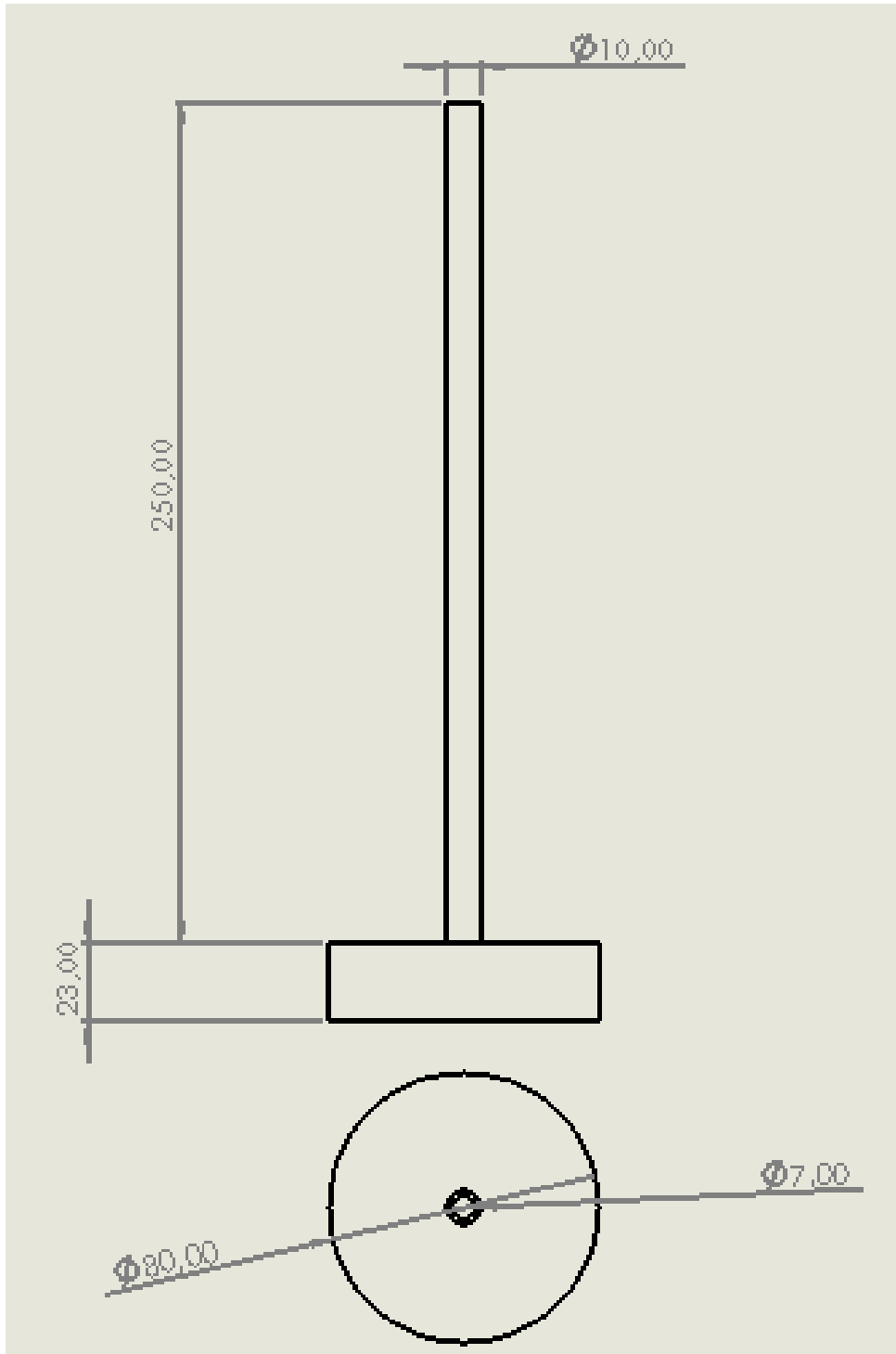


Figure 48: Stodola Green

7.2 Ch.4

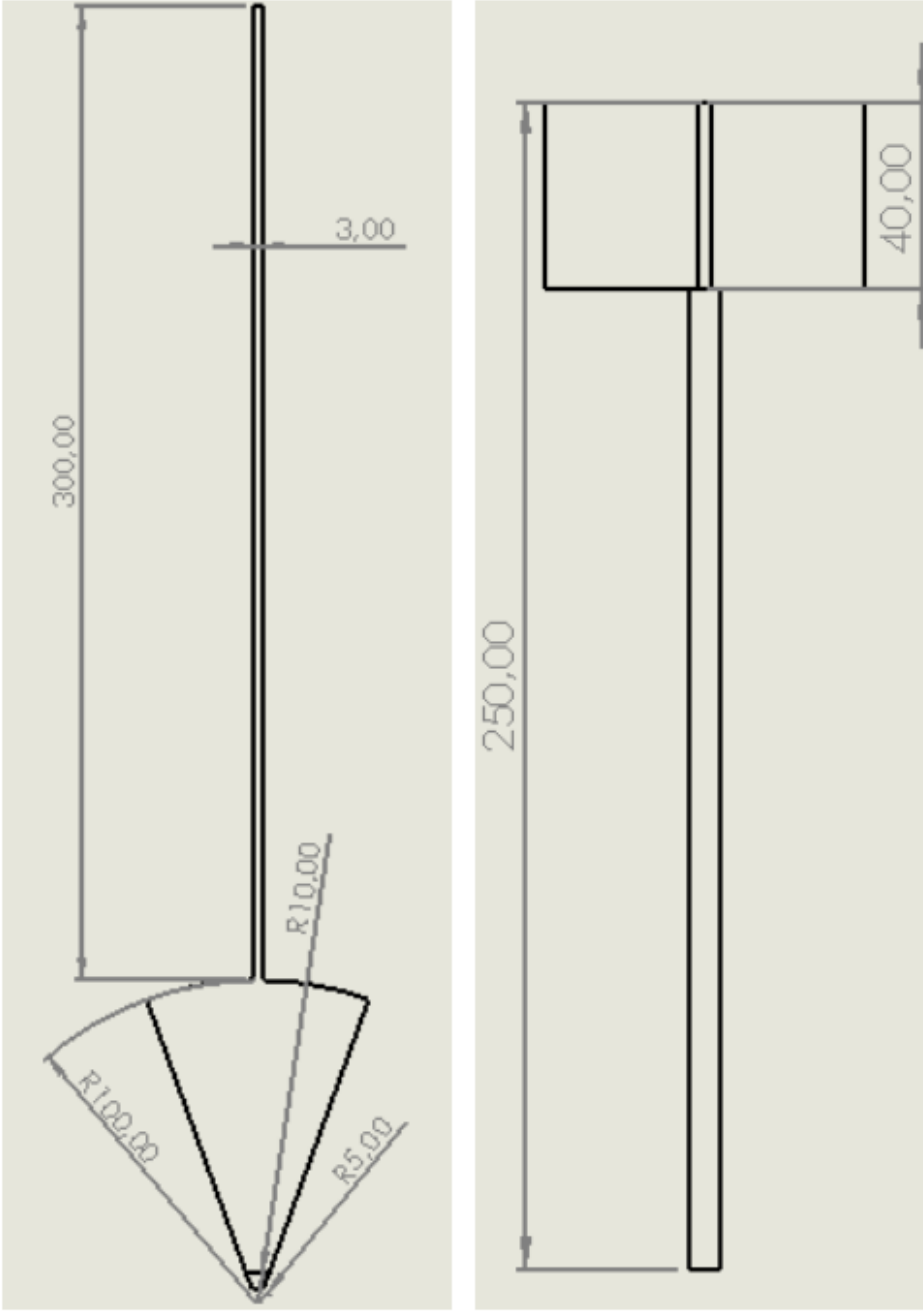


Figure 49: Bladed disc shaft assembly dimensions

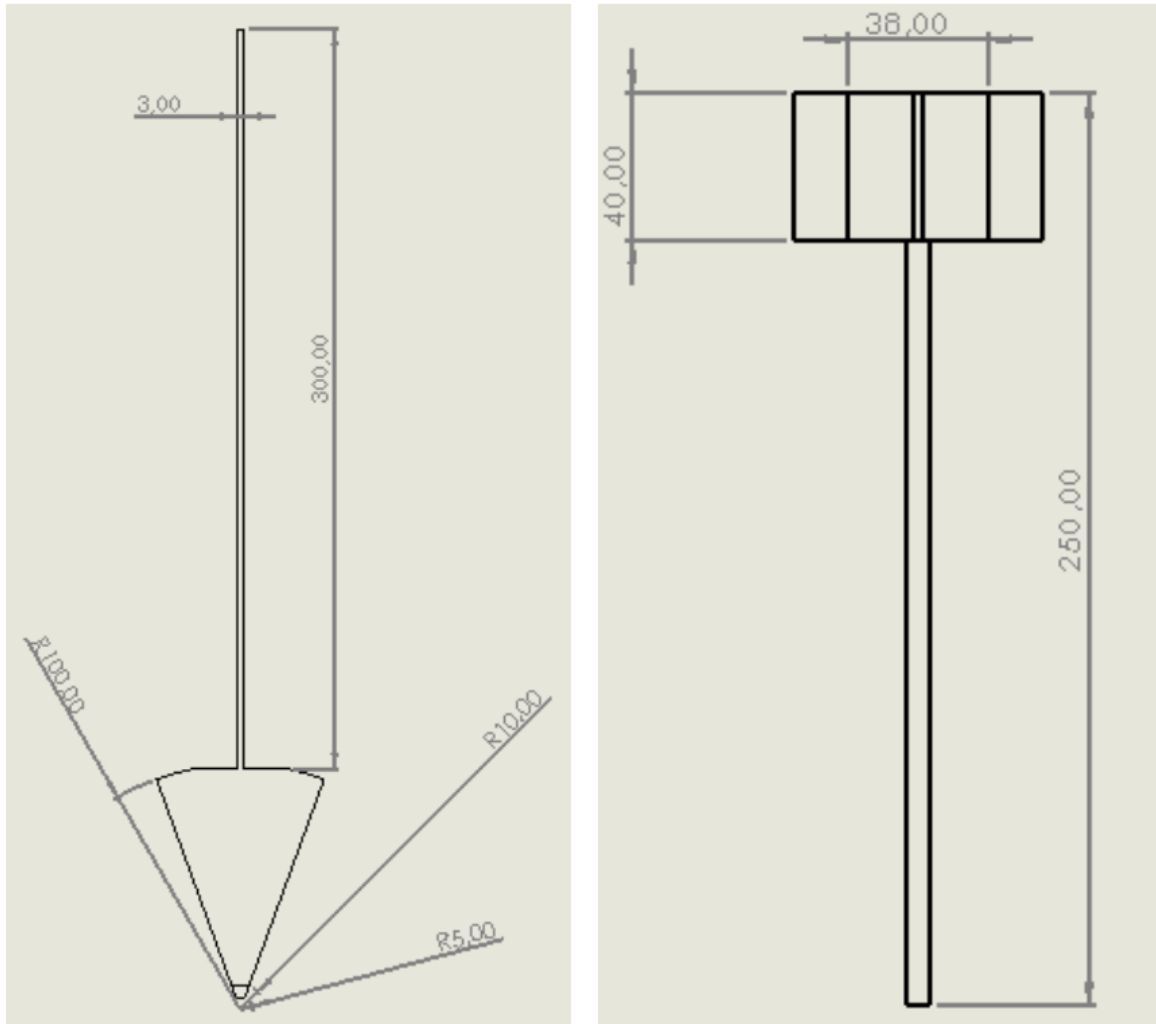


Figure 50: Bladed disc modified shaft assembly dimensions

7.2.1 Solution routine for the pre-stressed rotordynamic analysis of the bladed disc-shaft assembly

This routine solution holds for all the rotordynamic analysis to which apply the centrifugal stiffening effect, the gyroscopic effect, the spin softening effect IN THE LINEAR FIELD. If you just copy the solution in the *Ansys APDL* command bar, it should work. Remember always to check the differences between each version of the software (this routine works for the 2016 version). '!' symbol is needed to report something as comment in *Ansys APDL*. If you want to find examples about rotordynamics in *Ansys Mechanical APDL* you should check the software 'HELP' in the Rotordynamic section.

```

1
2 /prep7
3 !define materials
4 !select the element
5 !mesh the geometry
6 !set the constraints
7
8 ! set the analysis initial conditions:

```

```

9 spin=1400 ! in rad/s
10 nbstep = 28 !number of steps into which divide the analysis
11 dspin = spin/(nbstep-1)! speed increment
12 *dim,spins,,nbstep !creation of the vector of the speeds
13 *vfill,spins,ramp,0.,dspin !definition of the values of
14 !the spin vector through a ramp function
15 spins(1) = 0.1 ! non zero to ease the
16 !Campbell diagram sorting
17
18 *do,iloop,1,nbstep !do loop which solves firstly the static
19 !analysis which allows to build the geometrical
20 !stiffening matrix and the spin softening one
21 /solu !solution of the static analysis
22 antype,static
23 rescontrol,linear ! Enable file writing for
24 !a subsequent linear perturbation
25
26 coriolis,on ! Coriolis effect is On
27 !To note that the default reference frame
28 !to solve the analysis is the rotating one
29
30 omega,,spins(iloop) !Imposition of the rotational speed
31 !for the centrifugal force calculation\\
32
33 campbell,rstp
34 solve !solution of the static analysis
35 finish
36
37 /solu !Perform a restart in order to
38 !insert in the modal analysis
39 the matrices coming from the previous step
40 !(Geometric stiffness, spin softening)
41
42 antype,static, restart,,,perturb
43 ! Perform a static restart from the last
44 !load step and substep of the previous static solve
45
46 perturb, modal,,, INERKEEP
47
48 solve, elform ! Reform element matrices
49
50 modopt,damp,40,,,on ! selection of the
51 !solver an the number of modes to extract
52
53 mxpand,40 !Number of modes to expand
54
55 coriolis,on ! Coriolis effect On (to constitute
56 !the gyroscopic matrix) in the rotating reference frame
57
58 omega,,spins(iloop) !Assignment of the
59 !rotational speed to the modal analysis
60 !in order to solve a rotordynamic analysis
61
62 solve
63 finish
64 *enddo
65 /OUTPUT,freq_rot_blisc,txt
66 finish

```

```
67 ! *** Campbell diagram section in order to
68 !create a picture of the campbell and
69 !an automatic collection of its frequencies
70 !on the file freqrotblisc.txt
71 /post1
72 file,,rstp
73 /show,JPEG
74 plcamp,,rpm !plot the campbell with rotational speed in rpm
75 prcamp,,rpm ! save the frequencies
76 !of the campbell the text file
77 finish
78 /show,CLOSE
```

Listing 5: Stodola-Green lumped model assembly matrix function

References

- [1] Valentina Ruffini, Christoph W Schwingshackl, and Jeffrey S Green. “Prediction capabilities of Coriolis and gyroscopic effects in current finite element software”. In: *Proceedings of the 9th IFToMM International Conference on Rotor Dynamics*. Springer. 2015, pp. 1853–1862 (cit. on pp. 1, 2, 13–16, 21, 22, 24, 41, 42).
- [2] Erik Swanson, Chris D Powell, and Sorin Weissman. “A practical review of rotating machinery critical speeds and modes”. In: *Sound and vibration* 39.5 (2005), pp. 16–17 (cit. on p. 4).
- [3] Giancarlo Genta. *Dynamics of rotating systems*. Springer Science & Business Media, 2007 (cit. on pp. 6, 11, 12, 18, 25, 31).
- [4] D L_ Thomas. “Dynamics of rotationally periodic structures”. In: *International journal for numerical methods in engineering* 14.1 (1979), pp. 81–102 (cit. on pp. 9, 10).
- [5] G Genta and M Silvagni. “Three-dimensional fem rotordynamics and the so-called centrifugal softening of rotors”. In: *Atti dell’Accademia delle Scienze di Torino (to be published)* (2012) (cit. on p. 25).
- [6] M Aslan, O Guler, K Cava, U Alver, and E Yuceloglu. “An Investigation on the Mechanical Properties of the Sandwich Panel Composites”. In: *2nd International Defense Industry Symposium Science Board, Kirikkale, Turkey, April. 2017*, pp. 6–8 (cit. on p. 34).

8 RINGRAZIAMENTI

Ultimo ma non ultimo vorrei provare a ringraziare tutti quelli che mi hanno sostenuto e aiutato nel mio percorso accademico, e non, in questi anni. Partendo dal lato accademico vorrei ringraziare la Professoressa Teresa Berruti, mia relatrice e caposaldo durante lo sviluppo di questo elaborato. Il suo è stato un aiuto sicuro sul quale poter contare, cosa che in questi anni universitari non è mai stato scontato da parte dei professori. La professionalità e la competenza mi hanno portato a superare delle avversità che fino a qualche tempo fa avrei fatto anche solo fatica ad affrontare. Ringrazio inoltre la Dottoressa Valentina Ruffini che, col suo prezioso aiuto gratuito, mi ha dato una mano a superare le inconvenienze tecniche date dall'inesperienza oltre che avermi impartito una lezione di umanità. Ringrazio il Dottor Matteo Sorrenti che, oltre che un amico, è stato fonte di ispirazione e grande supporto nell'affrontare ancora una volta gli svariati problemi tecnici.

Voglio ancora ringraziare i miei genitori che mi hanno sempre dato il supporto necessario ai miei studi senza farmi mancare nulla. Insieme a mia Sorella Elisa hanno sempre cercato di spingermi a fare il meglio possibile ed è anche grazie a loro se sono riuscito a raggiungere questo traguardo. Ancora, ringrazio i miei Nonni Aleardo, Paola, Carmelo e Giuseppina, da i quali ho ereditato sicuramente molto e, che sempre mi accompagnano e si interessano di quel che faccio.

Un pensiero speciale agli amici di sempre Marco, Andrea, Giuseppe, Pietro, Federico, Andrea, Anastasia, Ilaria, Elena: grazie per avermi sopportato e supportato in questi anni, grazie per essermi stati d'esempio e per insegnarmi sempre qualcosa di nuovo!

Un grazie a Simone, Elia, Luca, Umberto, Matteo, per avermi strappato sorriso e avermi trascinato in avanti quando lo sconforto mi invadeva e, senza i quali probabilmente non sarei neanche andato oltre Analisi 1.

Un grazie alla mia seconda famiglia Torinese: Paolo, Nicola, Michele, Luca che mi hanno fatto sempre sentire a casa durante i risotti, le patate e il tanto pollo mangiati insieme.

Un grazie ancora a Patti, Fabietto, Giosuè, Davide, Lorenzo per aver condiviso con me le nostre passioni e avermi farmi conoscere un po' di più il Piemonte!

Un grazie al mio amico e collega Mike per tutte le ore di lezione e pranzo trascorse insieme.

Un grazie a tutte le persone importati che mi hanno insegnato qualcosa durante questo percorso. Non smettete di condividere le vostre idee e la vostra esperienza con gli altri perchè sono fonte di ispirazione e di crescita.

Un grazie alle tante persone che si sono trovate sulla mia strada in questi anni: vi porto tutti nel cuore e vi ricordo.